Summer 5-2017

Analytic Solutions for the Crack-Tip Plastic Zone under Mixed Mode Loading Conditions

Jason Ivey
University of New Mexico

Jason Ivey

Candidate

Mechanical Engineering

Department

This thesis is approved, and it is acceptable in quality and form for publication:

Approved by the Thesis Committee:

Tariq Khraishi , Chairperson

Mehran Tehrani

Yu-Lin Shen

ANALYTIC SOLUTIONS FOR THE CRACK-TIP PLASTIC ZONE RADIUS UNDER MIXED MODE LOADING CONDITIONS

by

JASON IVEY

BACHELORS OF SCIENCE
MECHANICAL ENGINEERING
UNIVERSITY OF NEW MEXICO
2014

THESIS

Submitted in Partial Fulfillment of the
Requirements for the Degree of

Master of Science
Mechanical Engineering

The University of New Mexico
Albuquerque, New Mexico

July 2017

Analytic Solutions for the Crack-Tip Plastic Zone Radius Under Mixed Mode Loading Conditions

By

Jason Ivey

B.S., Mechanical Engineering, University of New Mexico, 2014
M.S., Mechanical Engineering, University of New Mexico, 2017

Abstract

Analytic solutions for the plastic region surrounding a crack tip are derived under mixed mode I/II and mixed mode I/II/III loading conditions for an elastic-plastic solid with a semi-infinite crack. Both the Von Mises and Tresca yield criteria are applied. Additionally, plane stress and plane strain assumptions are included when applicable. The results show a strong dependence on the ratio of the stress intensity factors for each loading mode. It is shown that the plastic zone area given by the Tresca yield criterion is larger than that given by the Von Mises yield criterion. Lastly, it is investigated whether or not there is a correlation between the crack initiation angle predicted by the R-criterion (Khan and Khraisheh (2004)) and the principal stress directions.

TABLE OF CONTENTS

Introduction:

An important area of focus in fracture mechanics is the region surrounding a crack-tip. Knowing how this region behaves under loading can help predict not only if a crack will propagate, but can also help predict in which direction it will grow. To do this, both the size and shape of the plastic deformation radius around the crack-tip is found. Work on the plastic zone can be traced back to Irwin (1957) and Dugdale (1960). Banks and Garlick (1984) and Guerra-Rosa et al. (1984) presented analytic solutions for the plastic zone boundary using the Von Mises yield criterion for individual modes of loading. Additional work for individual loading modes has been done by Jing (2003, 2004) and Unger (1990), with the former investigating all three modes, and the later investigating mode III only.

The first to study crack initiation angles under mixed mode loading in the presence of an angled crack were Erdogan and Sih (1963). They presented the maximum tangential stress criterion, a widely-used theory for crack growth. Khan and Khraisheh (2004) continued the work with angled cracks by presenting a new growth criterion, called the R-criterion. They theorized the crack will grow toward the minimum plastic zone radius based on the minimum plastic work needed to create cracked surfaces. Theocaris and Andrianopolous (1982) presented the T-criterion, which uses a critical dilatational strain value to find the critical load at which a crack will propagate. Yehia (1991) modified this work by theorizing that the critical fracture load occurs at a critical value of the plastic region, naming it the Y-criterion. Additional mixed mode loading work has been presented by Iida and Kobayashi (1969) and Golos and Wasiluk (2000).

Another method that has been used to determine the plastic zone is the finite element method (FEM). Dodds et al.(1991) and Mishra and Parida (1985) both presented work on the plastic zone using FEM. Dodds showed the effects that strain hardening can have on the plastic zone size, whereas Mishra and Parida determined that the plastic zone size given by the Tresca yield criterion is larger than that given by the Von Mises yield criterion. Both assume an elastic-plastic material. Baxevanis et al. (2012) used a pseudoelastic shape memory alloy (SMA) under the plane strain assumption, and compared results obtained using FEM with those utilizing the more traditional elastic-plastic material. It was found that the plastic zone size of a SMA is an order of magnitude smaller than that of an elastic-plastic material.

Additionally, some effort has been made to create experimental results that can be used to test the accuracy of analytic models. Theocaris et al. (1982), and Kong et al. (1995) both presented data gained from uniaxial tension tests. In the case of Theocaris et al., a ductile material was used to evaluate the T-criterion, which states that small crack inclination angles must have propagation angles larger than 90°. Kong et al. used the maximum triaxial stress to determine the crack initiation angle, and found that the experimental results accurately described the predicted results. Although compression is not used for crack growth often, Vallejo (1987) obtained experimental data using uniaxial compression tests.

For mixed mode loading, the only criterion seen used in analytic work to find the plastic zone radius, to the knowledge of this author, is the Von Mises yield criterion. Additionally, no analytic solutions could be found for mixed mode loading other than mixed mode I/II. This paper presents analytic solutions for mixed modes I/II, I/III, II/III,

and I/II/III, although focusing on mixed modes I/II and I/II/III. Additionally, solutions are presented for both the Von Mises and Tresca yield criteria, with the later including the Invariant form and the principal stress form.

Individual Mode Stress State Definitions:

The stress components under each mode of loading are given in equations (1) through (13). As Irwin (1957) suggested, like stress components from separate applied loads on a single object can simply be added together, even when multiple types of tearing modes are present. Therefore, from the superposition process, a single term can be obtained for each stress component used in a given yield criterion.

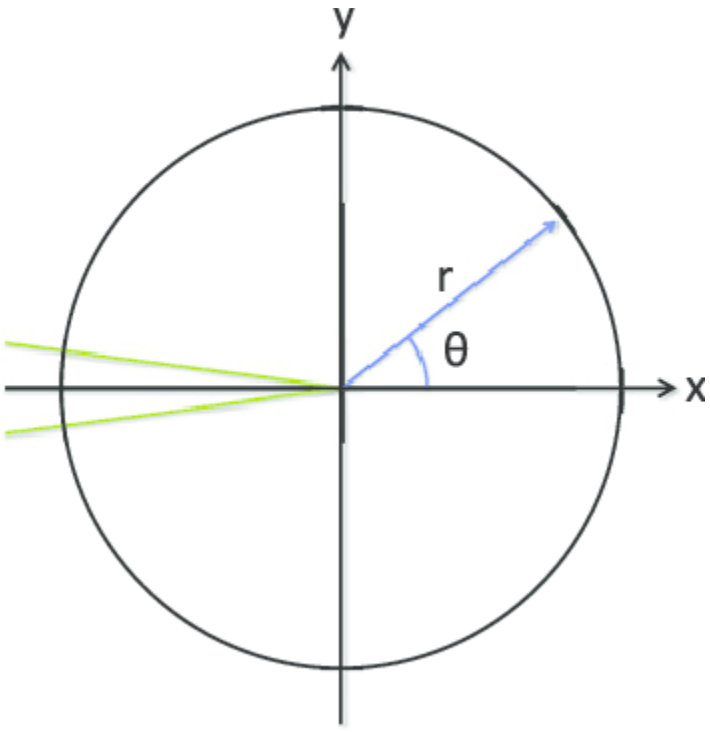

Figure 0 Crack-Tip location relative to polar and Cartesian coordinate systems

Mode I stress states

$$\sigma_{xx} = \frac{K_I}{\sqrt{2\pi r}} \cos\left(\frac{\theta}{2}\right)\left(1 - \sin(2\theta)\sin\left(\frac{3\theta}{2}\right)\right) \qquad (1)$$

$$\sigma_{yy} = \frac{K_I}{\sqrt{2\pi r}} \cos\left(\frac{\theta}{2}\right)\left(1 + \sin(2\theta)\sin\left(\frac{3\theta}{2}\right)\right) \quad (2)$$

$$\sigma_{xy} = \frac{K_I}{\sqrt{2\pi r}} \cos\left(\frac{\theta}{2}\right)\sin\left(\frac{\theta}{2}\right)\sin\left(\frac{3\theta}{2}\right) \quad (3)$$

$$\sigma_{xz} = \sigma_{yz} = 0 \quad (4)$$

$$\sigma_{zz} = \begin{cases} 0 & (Plane\ Stress) \\ \nu(\sigma_{xx} + \sigma_{yy}) & (Plane\ Strain) \end{cases} \quad (5)$$

Mode II stress states

$$\sigma_{xx} = -\frac{K_{II}}{\sqrt{2\pi r}} \sin\left(\frac{\theta}{2}\right)\left(2 + \cos\left(\frac{\theta}{2}\right)\cos\left(\frac{3\theta}{2}\right)\right) \quad (6)$$

$$\sigma_{yy} = \frac{K_{II}}{\sqrt{2\pi r}} \sin\left(\frac{\theta}{2}\right)\cos\left(\frac{\theta}{2}\right)\cos\left(\frac{3\theta}{2}\right) \quad (7)$$

$$\sigma_{xy} = \frac{K_{II}}{\sqrt{2\pi r}} \cos\left(\frac{\theta}{2}\right)\left(1 - \sin\left(\frac{\theta}{2}\right)\sin\left(\frac{3\theta}{2}\right)\right) \quad (8)$$

$$\sigma_{xz} = \sigma_{yz} = 0 \quad (9)$$

$$\sigma_{zz} = \begin{cases} 0 & (Plane\ Stress) \\ \nu(\sigma_{xx} + \sigma_{yy}) & (Plane\ Strain) \end{cases} \quad (10)$$

Mode III stress states

$$\sigma_{xx} = \sigma_{yy} = \sigma_{zz} = \sigma_{xy} = 0 \quad (11)$$

$$\sigma_{xz} = -\frac{K_{III}}{\sqrt{2\pi r}} \sin\left(\frac{\theta}{2}\right) \quad (12)$$

$$\sigma_{yz} = \frac{K_{III}}{\sqrt{2\pi r}} \cos\left(\frac{\theta}{2}\right) \quad (13)$$

Yield Criteria Definitions:

The plastic zone size can be determined by using one of several yielding criteria, including the Von Mises criterion, the Tresca invariant criterion, and the Tresca principal stress criterion. The Von Mises criterion is defined as:

$$\sigma_e = \frac{1}{\sqrt{2}}\Big(\big(\sigma_{xx}-\sigma_{yy}\big)^2 + \big(\sigma_{yy}-\sigma_{zz}\big)^2 + (\sigma_{zz}-\sigma_{xx})^2 + 6\big(\sigma_{xy}^2+\sigma_{xz}^2+\sigma_{yz}^2\big)\Big)^{1/2} \quad (14)$$

Yielding occurs when $\sigma_e=\sigma_{ys}$, where σ_e is the effective stress and σ_{ys} is the yield stress under uniaxial tension.

The Tresca invariant-form yield criterion is defined as:

$$4J_2^3 - 27J_3^2 - 36k^2J_2^2 + 96k^4J_2 - 64k^6 = 0 \quad (15)$$

J_2 and J_3 are invariants from the deviatoric stress tensor, and $k= \sigma_{ys}/2$, which is the yield stress under shearing conditions. J_2 is given as

$$J_2 = \frac{1}{6}\Big(\big(\sigma_{xx}-\sigma_{yy}\big)^2 + \big(\sigma_{yy}-\sigma_{zz}\big)^2 + (\sigma_{zz}-\sigma_{xx})^2 + 6\big(\sigma_{xy}^2+\sigma_{xz}^2+\sigma_{yz}^2\big)\Big) \quad (16)$$

and J_3 is given as

$$J_3 = \det\begin{bmatrix} \frac{2\sigma_{xx}-\sigma_{yy}-\sigma_{zz}}{3} & \sigma_{xy} & \sigma_{xz} \\ \sigma_{yx} & \frac{2\sigma_{yy}-\sigma_{xx}-\sigma_{zz}}{3} & \sigma_{yz} \\ \sigma_{zx} & \sigma_{zy} & \frac{2\sigma_{zz}-\sigma_{xx}-\sigma_{yy}}{3} \end{bmatrix} \quad (17)$$

The final yield criteria considered is the Tresca Principal Stress criteria, defined as :

$$\sigma^3 - I_1\sigma^2 - I_2\sigma - I_3 = 0 \quad (18)$$

I_1, I_2, and I_3 are given as:

$$I_1 = \sigma_{xx} + \sigma_{yy} + \sigma_{zz} \quad (19)$$

$$I_2 = \sigma_{xy}^2 + \sigma_{xz}^2 + \sigma_{yz}^2 - \sigma_{xx}\sigma_{yy} - \sigma_{xx}\sigma_{zz} - \sigma_{yy}\sigma_{zz} \quad (20)$$

$$I_3 = \sigma_{xx}\sigma_{yy}\sigma_{zz} + 2\sigma_{xy}\sigma_{xz}\sigma_{yz} - \sigma_{xx}\sigma_{yz}^2 - \sigma_{yy}\sigma_{xz}^2 - \sigma_{zz}\sigma_{xy}^2 \quad (21)$$

After solving for the principal stresses, either

$$\frac{\sigma_1 - \sigma_2}{2} = k \quad (22) \quad or \quad \frac{\sigma_1 - \sigma_3}{2} = k \quad (23) \quad or \quad \frac{\sigma_2 - \sigma_3}{2} = k \quad (24)$$

is used to determine when yielding occurs.

Primary Work

Mixed Mode I/II

Before similar components of the stress equations (1) through (5) and (6) through (10) can be combined, it must be noted that two separate stress intensity factors are present. The plastic zone radii are typically normalized with respect to the stress intensity factor, along with several other variables, thereby creating a non-dimensional value for each radius. To maintain a non-dimensional value, a ratio of the two stress intensity factors is created so a single factor may be used for normalization. The ratio is defined as:

$$Kr_1 = \frac{K_{II}}{K_I} \qquad (25)$$

Adding equations (1) through (5) with (6) through (10), and combing the resulting equations with (25) gives a final set of stress values.

$$\sigma_{xx} = \frac{K_I}{\sqrt{2\pi r}}\cos\left(\frac{\theta}{2}\right)\left(1 - \sin(2\theta)\sin\left(\frac{3\theta}{2}\right)\right) - \frac{K_I Kr_1}{\sqrt{2\pi r}}\sin\left(\frac{\theta}{2}\right)\left(2 + \cos\left(\frac{\theta}{2}\right)\cos\left(\frac{3\theta}{2}\right)\right) \qquad (26)$$

$$\sigma_{yy} = \frac{K_I}{\sqrt{2\pi r}}\cos\left(\frac{\theta}{2}\right)\left(1 + \sin(2\theta)\sin\left(\frac{3\theta}{2}\right)\right) + \frac{K_I Kr_1}{\sqrt{2\pi r}}\sin\left(\frac{\theta}{2}\right)\cos\left(\frac{\theta}{2}\right)\cos\left(\frac{3\theta}{2}\right) \qquad (27)$$

$$\sigma_{xy} = \frac{K_I}{\sqrt{2\pi r}}\cos\left(\frac{\theta}{2}\right)\sin\left(\frac{\theta}{2}\right)\sin\left(\frac{3\theta}{2}\right) + \frac{K_I Kr_1}{\sqrt{2\pi r}}\cos\left(\frac{\theta}{2}\right)\left(1 - \sin\left(\frac{\theta}{2}\right)\sin\left(\frac{3\theta}{2}\right)\right) \qquad (28)$$

$$\sigma_{xz} = \sigma_{yz} = 0 \qquad (29)$$

$$\sigma_{zz} = \begin{cases} 0 & (Plane\ Stress) \\ \nu(\sigma_{xx} + \sigma_{yy}) & (Plane\ Strain) \end{cases} \qquad (30)$$

Von Mises

Equations (26) through (30) are substituted into equation (14), following which the radius of the plastic zone can be directly solved for. Finally, the radius is normalized with respect to the yield stress and the stress intensity factor under mode I loading as shown in equation (31).

$$r(\theta) = \frac{R(\theta)\left(\pi\sigma_{ys}^2\right)}{K_I^2} \quad (31)$$

The non-dimensional results for the plastic zone are

$$r(\theta) = \frac{1}{16}\big(7 + 19Kr_1^2 + (-3 + 9Kr_1^2)\cos 2\theta - 8Kr_1 \sin\theta$$
$$+ 4\cos\theta\,(1 - Kr_1^2 + 6Kr_1 \sin\theta)\big) \quad (32)$$

for plane stress, and

$$r(\theta) = \frac{1}{16}(7 + 16(-1+\nu)\nu + Kr_1^2(19 + 16(-1+\nu)\nu)$$
$$- 4(-1 + Kr_1^2)(1-2\nu)^2\cos\theta + (-3 + 9Kr_1^2)\cos 2\theta$$
$$+ 8Kr_1(-(1-2\nu)^2 + 3\cos\theta)\sin\theta \quad (33)$$

for plane strain. All mathematical results herein were obtained using the symbolic engine of Mathematica software.

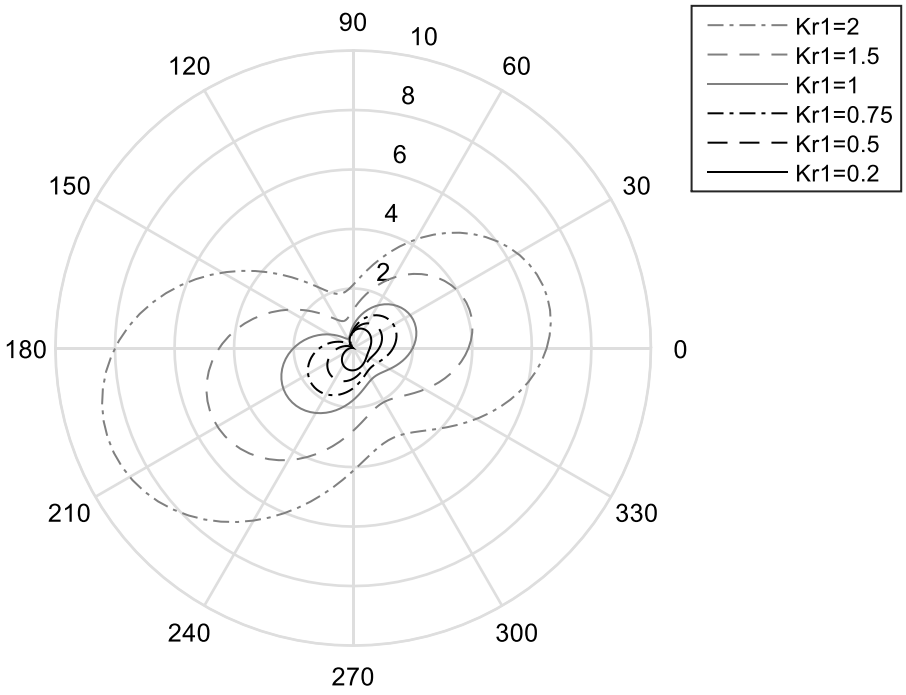

Figure 1 Mixed Mode I/II Von Mises: Plane Stress Plastic Zone Radius

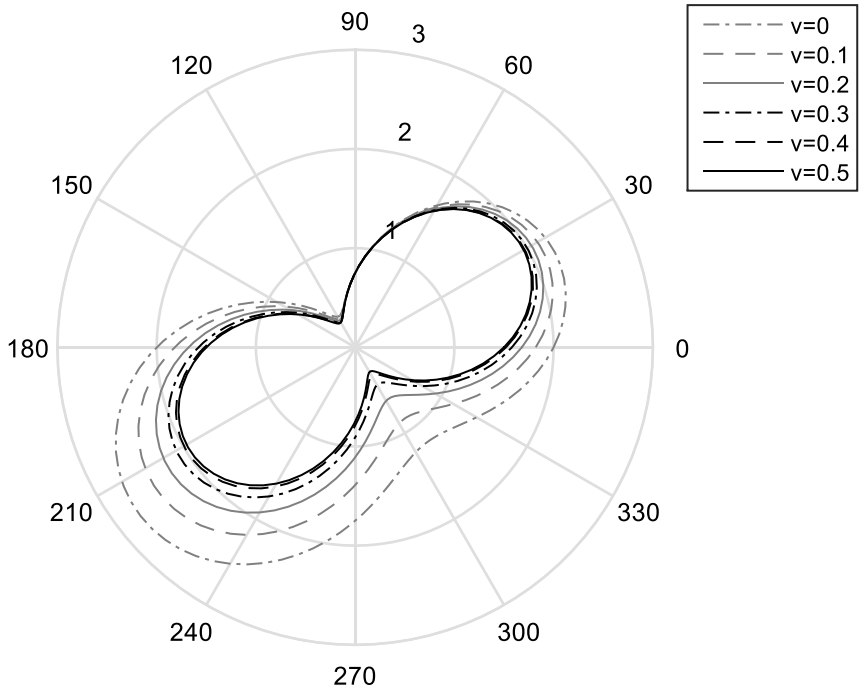

Figure 2 Mixed Mode I/II Von Mises: Plane Strain Plastic Zone Radius Kr1=1

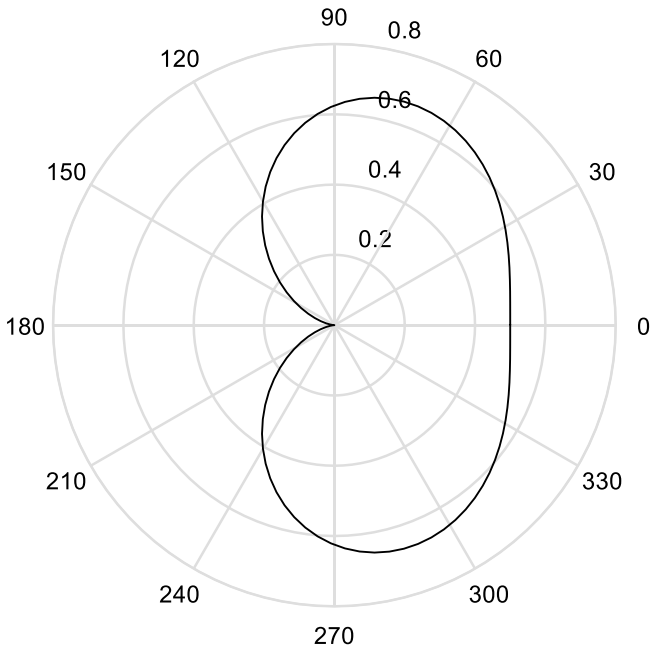

Figure 3 Kidney-Shape representing pure mode I

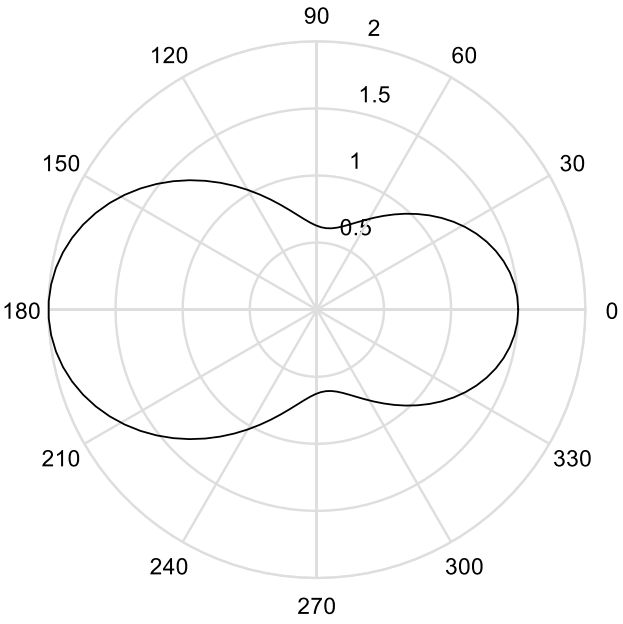

Figure 4 Peanut-Shape representing pure mode II

Figure (1) shows the plastic zone shape under the plane stress condition for six stress intensity factor ratios. In this and all following figures with polar coordinates, the crack extends from the left of the horizontal line to the center of the figure. There are

three visible trends that can easily be seen. First the plastic zone area increases as the K ratio increases. Second, the shape rotates clockwise with an increase in K ratio. Lastly, the shape changes. The larger K ratios are shaped like a peanut. As the ratio decreases, one side begins to flatten and the other side constricts, becoming more kidney shape. Examples of the peanut and kidney shapes can be seen in figures (3) and (4). This behavior is expected as it follows the transition from closer to pure mode II loading to closer to pure mode I loading as the K ratio decreases.

Figure (2) shows the plastic zone shape under the plane strain condition for a single stress intensity factor, Kr_1=1, and six Poisson's ratios. Two of three trends seen in figure (1) can be seen in figure (2). As the Poisson's ratio increases, the plastic zone shape changes from the more kidney shape, becoming more peanut-like in shape. Additionally, the plastic zone size decreases as the Poisson's ratio increases. Although not shown, it should also be noted that there is a rotation trend as well for a constant Poisson's ratio and changing stress intensity factor ratios.

Tresca Invariant

Equations (26) through (30) are combined with (15) through (17), giving a cubic equation for the radius in the form:

$$r^3 + a(\theta)r^2 + b(\theta)r + c(\theta) = 0 \quad (34)$$

The roots can be found analytically using the equations below.

$$p = \frac{3b - a^2}{3} \quad (35)$$

$$q = c + \frac{2a^3}{27} - \frac{ab}{3} \quad (36)$$

$$\cos\varphi = -\frac{q}{2\sqrt{\left(\frac{|p|}{3}\right)^3}} \quad (37)$$

There are three real roots if:

$$D = \left(\frac{p}{3}\right)^3 + \left(\frac{q}{2}\right)^2 < 0 \quad (38)$$

The three solutions are then in the form of:

$$r_1 = -\frac{a}{3} + 2\sqrt{\frac{|p|}{3}}\cos\frac{\varphi}{3} \quad (39)$$

$$r_2 = -\frac{a}{3} - 2\sqrt{\frac{|p|}{3}}\cos\frac{\varphi - \pi}{3} \quad (40)$$

$$r_3 = -\frac{a}{3} - 2\sqrt{\frac{|p|}{3}}\cos\frac{\varphi + \pi}{3} \quad (41)$$

For plane stress the roots are:

$$r_1 = \frac{f_1}{24}\left(1 + \cos\left(\frac{1}{3}ArcCos\left(\frac{-f_1^3 + f_2}{f_1^3}\right)\right)\right) \quad (42)$$

$$r_2 = \frac{f_1}{24}\left(1 - \cos\left(\frac{1}{3}\left(-\pi + ArcCos\left(\frac{-f_1^3 + f_2}{f_1^3}\right)\right)\right)\right) \quad (43)$$

$$r_3 = \frac{f_1}{24}\left(1 - \cos\left(\frac{1}{3}\left(\pi + ArcCos\left(\frac{-f_1^3 + f_2}{f_1^3}\right)\right)\right)\right) \quad (44)$$

where

$$f_1 = 7 + 19Kr_1^2 + (-3 + 9Kr_1^2)\cos 2\theta - 8Kr_1 \sin\theta + 4\cos\theta\,(1 - Kr_1^2 + 6Kr_1 \sin\theta) \quad (45)$$

$$f_2 = 864\cos\left(\frac{\theta}{2}\right)^4 (1 + Kr_1^2 + \cos\theta - 3Kr_1^2\cos\theta - 4Kr_1\sin\theta)(1 + 5Kr_1^2 + (-1 + 3Kr_1^2)\cos 2\theta + 4Kr_1\sin 2\theta) \qquad (46)$$

For plane strain the roots are:

$$r_1 = \frac{f_3}{24}\left(1 + \cos\left(\frac{1}{3}ArcCos\left(\frac{-f_3^3 + f_4}{f_3^3}\right)\right)\right) \qquad (47)$$

$$r_2 = \frac{f_3}{24}\left(1 - \cos\left(\frac{1}{3}\left(-\pi + ArcCos\left(\frac{-f_3^3 + f_4}{f_3^3}\right)\right)\right)\right) \qquad (48)$$

$$r_3 = \frac{f_3}{24}\left(1 - \cos\left(\frac{1}{3}\left(\pi + ArcCos\left(\frac{-f_3^3 + f_4}{f_3^3}\right)\right)\right)\right) \qquad (49)$$

where

$$f_3 = 7 + 16(-1 + \nu)\nu + Kr_1^2(19 + 16(-1 + \nu)\nu) - 4(-1 + Kr_1^2)(1 - 2\nu)^2\cos\theta + (-1 + 3Kr_1^2)\cos 2\theta + 8Kr_1((1 - 2\nu)^2 + 3\cos\theta)\sin\theta \qquad (50)$$

$$f_4 = 54(-3 + Kr_1^2 + 16(1 + Kr_1^2)\nu - 16(1 + Kr_1^2)\nu^2 + 4(-1 + Kr_1^2)(1 - 2\nu)^2\cos\theta + (-1 + 3Kr_1^2)\cos 2\theta + 8Kr_1((1 - 2\nu)^2 + \cos\theta)\sin\theta)^2\,(1 + 5Kr_1^2 + (-1 + 3Kr_1^2)\cos 2\theta + 4Kr_1\sin 2\theta) \qquad (51)$$

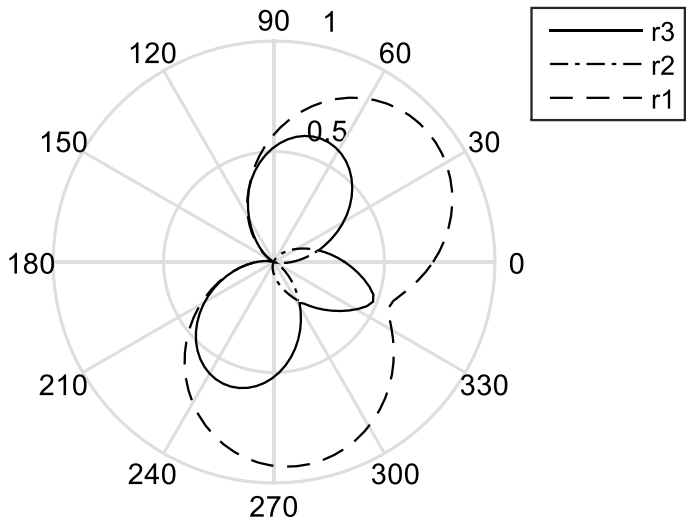

Figure 5 Mixed Mode I/II Tresca Invariant Form: Plane Stress Kr1=0.2

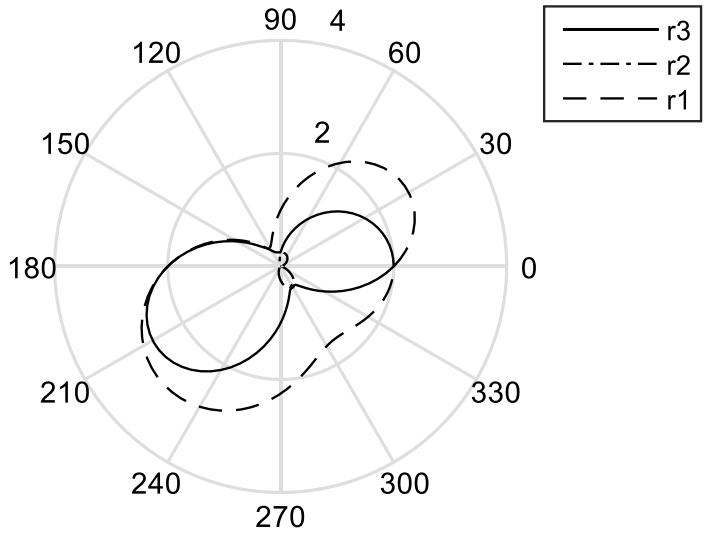

Figure 6 Mixed Mode I/II Tresca Invariant Form: Plane Stress Kr1=1

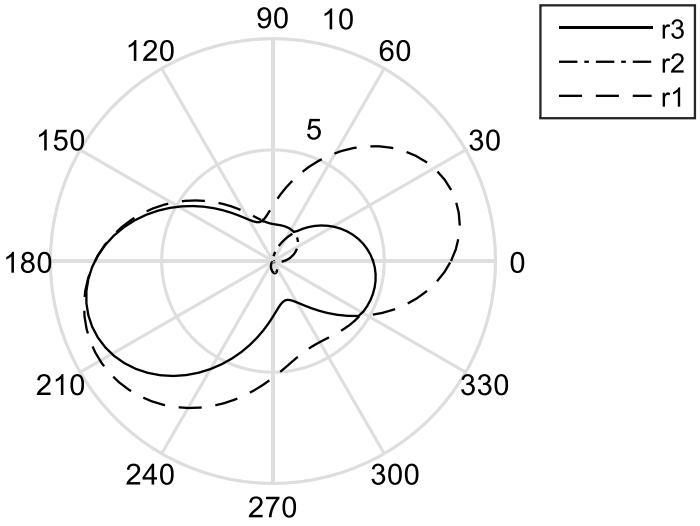

Figure 7 Mixed Mode I/II Tresca Invariant Form: Plane Stress Kr1=2

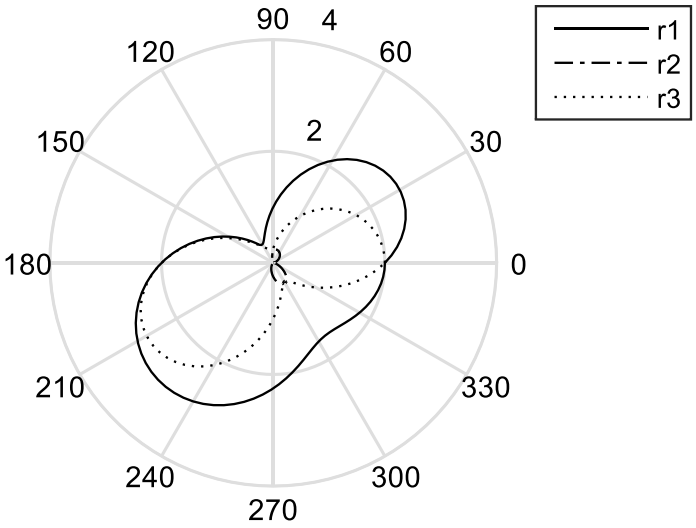

Figure 8 Mixed Mode I/II Tresca Invariant Form: Plane Strain v=0 Kr1=1

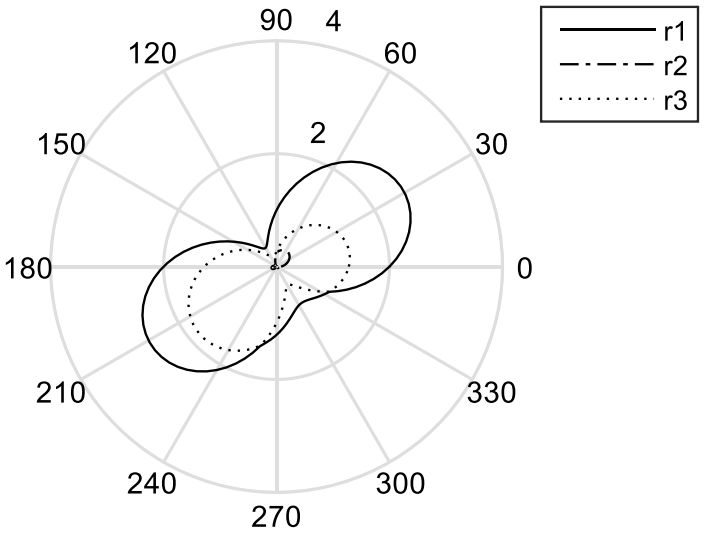

Figure 9 Mixed Mode I/II Tresca Invariant Form: Plane Strain v=0.2 Kr1=1

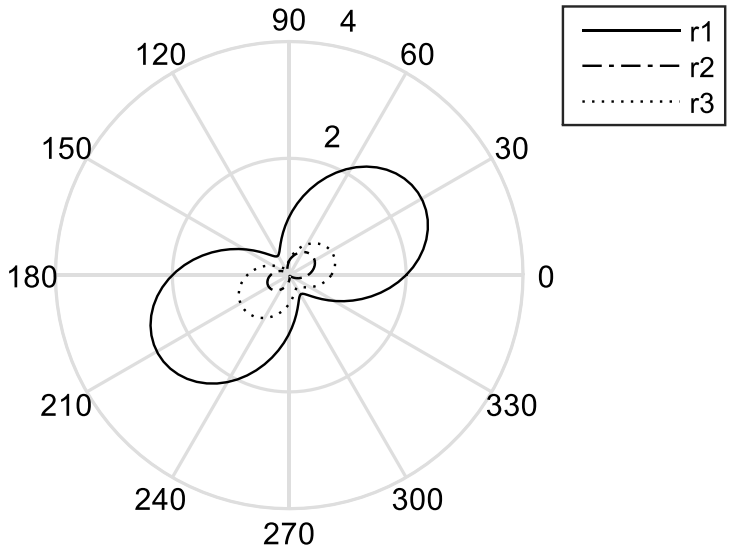

Figure 10 Mixed Mode I/II Tresca Invariant Form: Plane Strain v=0.4 Kr1=1

For any θ, the radius with the maximum value is used at that point. For all six figures shown above, r_1 is always largest, and thus is the only radius needed for analysis. Figures (5) through (7) show the results for the Tresca invariant form yield criterion using the plane stress assumption. As was seen in the results from the Von Mises yield criterion, the shape rotates from a more vertical position closer to a horizontal position as

the K ratio increases. Again, this coincides with the transition from mostly mode I loading to mostly mode II loading. A shape change similar to that seen in the Von Mises results is also present, but with an additional feature. As the mode II loading becomes more prevalent, an unexpected slope discontinuity appears. In figure (6) it occurs at θ=0°, and in figure (7) it occurs at θ=330°. When the shear loading starts to become dominant, the slope discontinuity becomes less severe. However, once the Poisson's ratio is introduced and increased, as seen in figures (8) through (10) for the plane strain assumption, this additional slope discontinuity starts to disappear.

Tresca Principal Stress

Using the Tresca Principal Stress criteria, equations (26) through (30) are combined with (18) through (21), yielding another cubic root. Using the same root formula seen in the Tresca Invariant Form criteria, the principal stresses are:

$$\sigma_1 = \frac{1}{6}\left(f_5 + \sqrt{f_6}\cos\left(\frac{1}{3}ArcCos\left(\frac{f_5 f_7}{\sqrt{{f_6}^3}}\right)\right)\right) \quad (52)$$

$$\sigma_2 = \frac{1}{6}\left(f_5 - \sqrt{f_6}\cos\left(\frac{1}{3}\left(-\pi + ArcCos\left(\frac{f_5 f_7}{\sqrt{{f_6}^3}}\right)\right)\right)\right) \quad (53)$$

$$\sigma_3 = \frac{1}{6}\left(f_5 - \sqrt{f_6}\cos\left(\frac{1}{3}\left(\pi + ArcCos\left(\frac{f_5 f_7}{\sqrt{{f_6}^3}}\right)\right)\right)\right) \quad (54)$$

where

$$f_5 = 2\sqrt{2}\left(\cos\frac{\theta}{2} - Kr_1 \sin\frac{\theta}{2}\right) \quad (55)$$

$$f_6 = 7 + 19Kr_1^2 + (-3 + 9Kr_1^2)\cos 2\theta - 8Kr_1 \sin\theta + 4\cos\theta\,(1 - Kr_1^2 + 6Kr_1 \sin\theta) \quad (56)$$

$$f_7 = 5 + 41Kr_1^2 + 9(-1 + 3Kr_1^2)\cos 2\theta + 8Kr_1 \sin\theta + 4\cos\theta\,(-1 + Kr_1^2 + 18Kr_1 \sin\theta) \quad (57)$$

for plane stress, and

$$\sigma_1 = \frac{1}{6}\left(f_8(1+\nu) + \sqrt{f_9}\cos\left(\frac{1}{3}ArcCos\left(-\frac{f_8 f_{10}(-1+2\nu)}{\sqrt{f_9^3}}\right)\right)\right) \quad (58)$$

$$\sigma_2 = \frac{1}{6}\left(f_8(1+\nu) - \sqrt{f_9}\cos\left(\frac{1}{3}\left(-\pi + ArcCos\left(-\frac{f_8 f_{10}(-1+2\nu)}{\sqrt{f_9^3}}\right)\right)\right)\right) \quad (59)$$

$$\sigma_3 = \frac{1}{6}\left(f_8(1+\nu) - \sqrt{f_9}\cos\left(\frac{1}{3}\left(\pi + ArcCos\left(-\frac{f_8 f_{10}(-1+2\nu)}{\sqrt{f_9^3}}\right)\right)\right)\right) \quad (60)$$

where

$$f_8 = 2\sqrt{2}\left(\cos\frac{\theta}{2} - Kr_1 \sin\frac{\theta}{2}\right) \quad (61)$$

$$f_9 = 7 + 16(-1+\nu) + Kr_1^2(19 - 16\nu + 16\nu^2) - 4(-1 + Kr_1^2)(1-2\nu)^2\cos\theta + 3(-1 + 3Kr_1^2)\cos 2\theta - 8Kr_1((1-2\nu)^2 - 3\cos\theta)\sin\theta \quad (62)$$

$$f_{10} = 5 - 16(-1+\nu)\nu + Kr_1^2(41 - 16(-1+\nu)\nu) + 4(-1 + Kr_1^2)(1-2\nu)^2\cos\theta + 9(-1 + 3Kr_1^2)\cos 2\theta + 8Kr_1((1-2\nu)^2 + 9\cos\theta)\sin\theta \quad (63)$$

for plane strain. It should be noted that, in some cases, functions (ex. f_1, f_2…) will be equal to each other. For example, f_1 and f_6 are equal, but are each written and labeled separately. This is done for the convenience of the reader since the instance where a function is repeated may be sufficiently far from its original occurrence.

After substituting these principal stress terms into equations (22) through (24), and then taking the maximum of the three equations, the plastic zone radius can be found. It should be noted that the radii shown in figures (11) and (12) are obtained numerically. In order to have a purely analytic radius, it must be known which principal stress criterion is dominant over a given range of θ. It can be shown that the value for σ_2 derived from the cubic root solutions in equations (39) through (41) will always be the smallest term. However, one must solve for the θ inside the φ shown in those equations to determine when which of the remaining principal stresses is the maximum. For mixed mode I/II, under plane stress, there are 9 distinct solutions for θ representing when one principal stress surpasses the other. Due to this large number of solutions, and the larger number that would exist when the Poisson's ratio and a second stress intensity factor are introduced, it was determined that an analytic solution for the principal stresses themselves is sufficient, and that the radii can be found numerically.

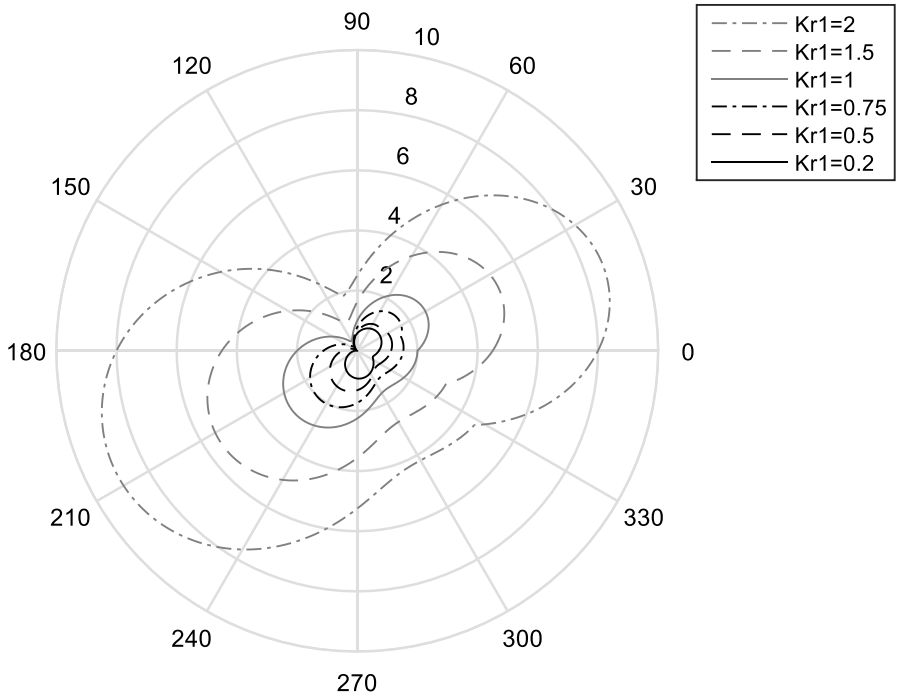

Figure 11 Mixed Mode I/II Tresca Principal Stress: Plane Stress

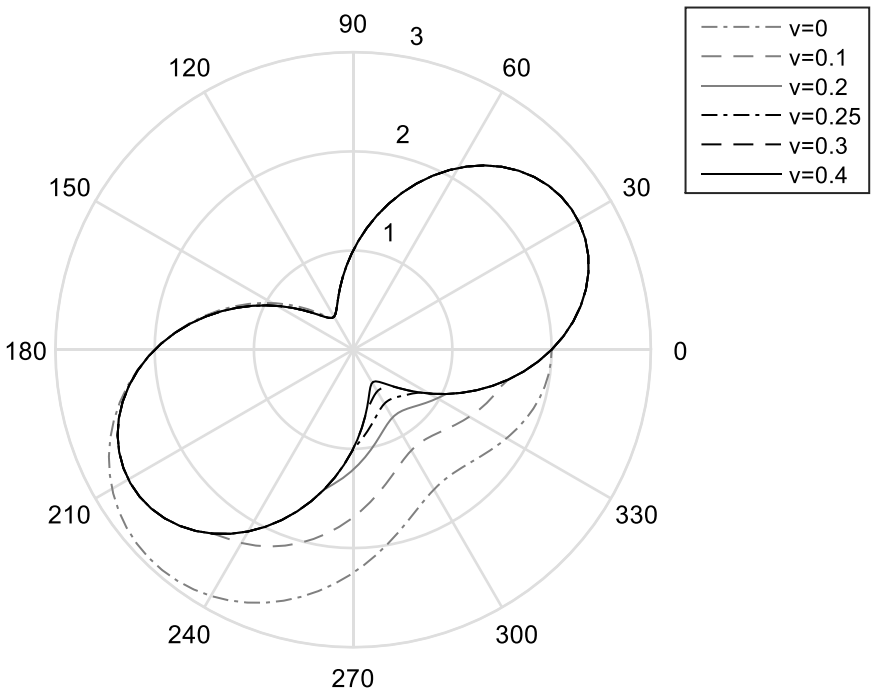

Figure 12 Mixed Mode I/II Tresca Principal Stress: Plane Strain Kr1=1

Figures (11) and (12) show the plastic zone shape under the plane stress and plane strain conditions, respectively, for the Tresca principal stress criterion. These match the outer radii in figures (5) through (10). This is expected as they use the same yield criterion, just using different methods. Figures (11) and (12) also more clearly show the behavior of the slope discontinuity discussed earlier.

Mode I/II/III

Similar to mixed mode I/II, mixed mode I/II/III contains more than one type of stress intensity factor. The same process is used to describe the stress states with respect to a single stress intensity factor, only in this case a second ratio must be introduced.

$$Kr_2 = \frac{K_{III}}{K_I} \qquad (64)$$

Another complication occurs due to the presence of the mode III loading, an out of plane type of loading. The plane stress condition becomes invalid, and the plane strain condition can no longer accurately describe a physical system. Any real system will lie somewhere in the middle, between a very thin plate (i.e. plane stress), and very thick plate (i.e. plane strain). The simplest way to account for this is to include a constant, C, in front of the Poisson's ratio (i.e. C ν instead of ν), and confine C to values between zero and one. In place of the constant and Poisson's ratio term, it makes sense that a single term, α, be used in its place.

$$\alpha = C\nu \quad (65)$$

Adding like stress components in equations (1) through (5) with (6) through (10) and (11) through (13), and then combining with equations (25), (64), and (65) gives:

$$\sigma_{xx} = \frac{K_I}{\sqrt{2\pi r}}\cos\left(\frac{\theta}{2}\right)\left(1 - \sin(2\theta)\sin\left(\frac{3\theta}{2}\right)\right) - \frac{K_I K r_1}{\sqrt{2\pi r}}\sin\left(\frac{\theta}{2}\right)\left(2 + \cos\left(\frac{\theta}{2}\right)\cos\left(\frac{3\theta}{2}\right)\right) \quad (66)$$

$$\sigma_{yy} = \frac{K_I}{\sqrt{2\pi r}}\cos\left(\frac{\theta}{2}\right)\left(1 + \sin(2\theta)\sin\left(\frac{3\theta}{2}\right)\right) + \frac{K_I K r_1}{\sqrt{2\pi r}}\sin\left(\frac{\theta}{2}\right)\cos\left(\frac{\theta}{2}\right)\cos\left(\frac{3\theta}{2}\right) \quad (67)$$

$$\sigma_{xy} = \frac{K_I}{\sqrt{2\pi r}}\cos\left(\frac{\theta}{2}\right)\sin\left(\frac{\theta}{2}\right)\sin\left(\frac{3\theta}{2}\right) + \frac{K_I K r_1}{\sqrt{2\pi r}}\cos\left(\frac{\theta}{2}\right)\left(1 - \sin\left(\frac{\theta}{2}\right)\sin\left(\frac{3\theta}{2}\right)\right) \quad (68)$$

$$\sigma_{xz} = -\frac{K_I\, K r_2}{\sqrt{2\pi r}}\sin\left(\frac{\theta}{2}\right) \quad (69)$$

$$\sigma_{yz} = \frac{K_I\, K r_2}{\sqrt{2\pi r}}\cos\left(\frac{\theta}{2}\right) \quad (70)$$

$$\sigma_{zz} = \alpha(\sigma_{xx} + \sigma_{yy}) \quad (71)$$

The processes for finding the plastic zone with each yield criteria under mixed mode I/II loading are repeated for the mixed mode I/II/III loading case, now using equations (66) through (71) as the stress components.

Von Mises

The plastic zone radius using the Von Mises criterion is found to be:

$$r = \frac{1}{16}(7 + 24Kr_2^2 + 16(-1+\alpha)\alpha + Kr_1^2(19 + 16(-1+\alpha)\alpha) - 4(-1 + Kr_1^2)(1-2\alpha)^2\cos\theta + (-3 + 9Kr_1^2)\cos 2\theta + 8Kr_1(-(1-2\alpha)^2 + 3\cos\theta)\sin\theta) \quad (72)$$

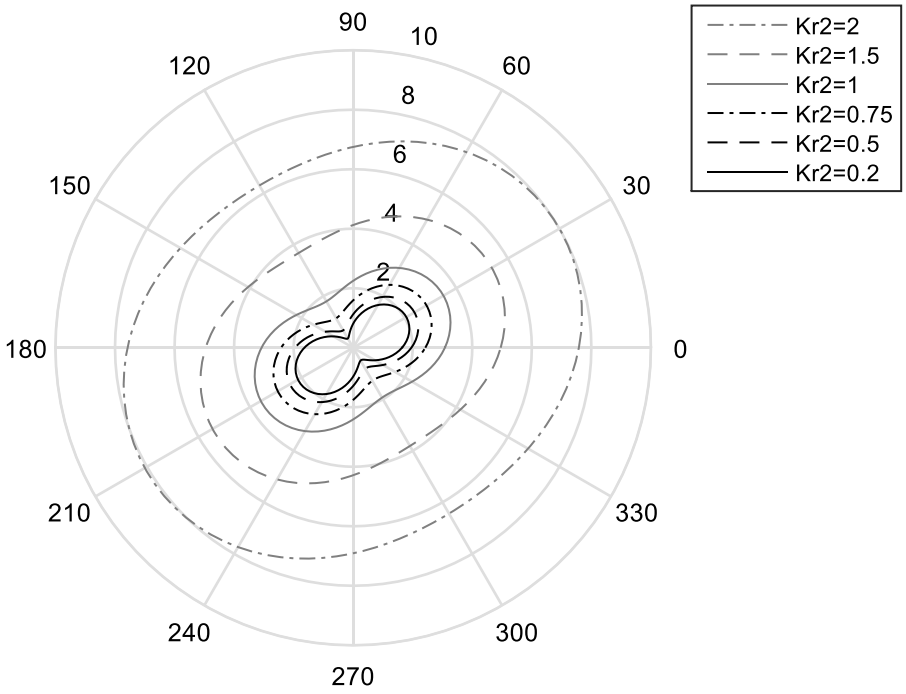

Figure 13 Mixed Mode I/II/III Von Mises Kr1=1, α=0.3

Figure (13) shows the results for mixed mode I/II/III loading using the Von Mises yield criterion. Single values for Kr1 and α were used, 1 and 0.3, respectively, so the effects of the second stress intensity factor ratio, Kr2, can be observed. Figure (13)

contains several of the same general forms of behavior seen in figure (1). As Kr2 increases, the radius becomes more circular as mode III loading becomes the more dominant form of loading. Additionally, the radius grows larger as Kr2 increase. There is no rotation with a change in Kr2 due to the fact that mode III loading is out-of-plane loading.

Tresca Invariant Form

Using the Tresca Invariant form yielding criterion, the radii are:

$$r_1 = \frac{f_{11}}{24}\left(1 + \cos\left[\frac{1}{3}ArcCos\left[\frac{-f_{11}^3 + 2\left({f_{11}}^3 + f_{12}{f_{13}}^2\right)}{{f_{11}}^3}\right]\right]\right) \quad (73)$$

$$r_2 = \frac{f_{11}}{24}\left(1 - \cos\left[\frac{1}{3}\left(-\pi + ArcCos\left[\frac{-f_{11}^3 + 2\left({f_{11}}^3 + f_{12}{f_{13}}^2\right)}{{f_{11}}^3}\right]\right)\right]\right) \quad (74)$$

$$r_3 = \frac{f_{11}}{24}\left(1 - \cos\left[\frac{1}{3}\left(\pi + ArcCos\left[\frac{-f_{11}^3 + 2\left({f_{11}}^3 + f_{12}{f_{13}}^2\right)}{{f_{11}}^3}\right]\right)\right]\right) \quad (75)$$

where

$$f_{11} = 7 + 24Kr_2^2 + 16(-1+\alpha)\alpha + Kr_1^2(19 + 16(-1+\alpha)\alpha) - 4(-1 + Kr_1^2)(1-2\alpha)^2\cos\theta + (-3 + 9Kr_1^2)\cos 2\theta + 8Kr_1(-(1-2\alpha)^2 + 3\cos\theta)\sin\theta \quad (76)$$

$$f_{12} = -8\left(\cos\frac{\theta}{2} - Kr_1\sin\frac{\theta}{2}\right)^2 \quad (77)$$

$$f_{13} = (-1-4\alpha)\left(5 + 18Kr_2^2 + 2\alpha(-7+4\alpha)\right) + Kr_1^2\left(-41 + 2\alpha\left(33 + 8\alpha(3-2\alpha)\right)\right) + 2(27Kr_2^2 - 2(1+2\alpha)^3 + 2Kr_1^2(-1+2\alpha)^3)\cos\theta + (-1+2\alpha)(9(-1+3Kr_1^2)\cos 2\theta + 8Kr_1((1-2\alpha)^2 + 9\cos\theta)\sin\theta) \quad (78)$$

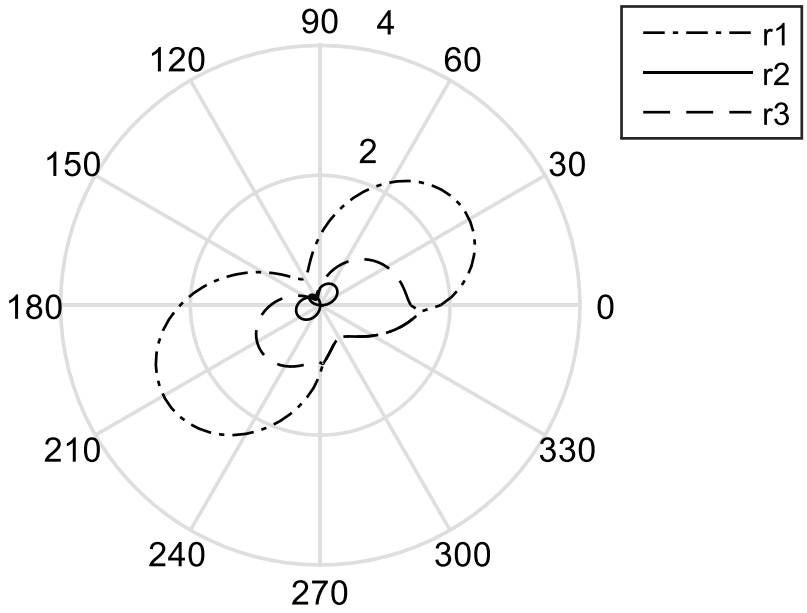

Figure 14 Mixed Mode I/II/III Tresca Invariant Form: Kr1=1, α=0.3, Kr2=0.2

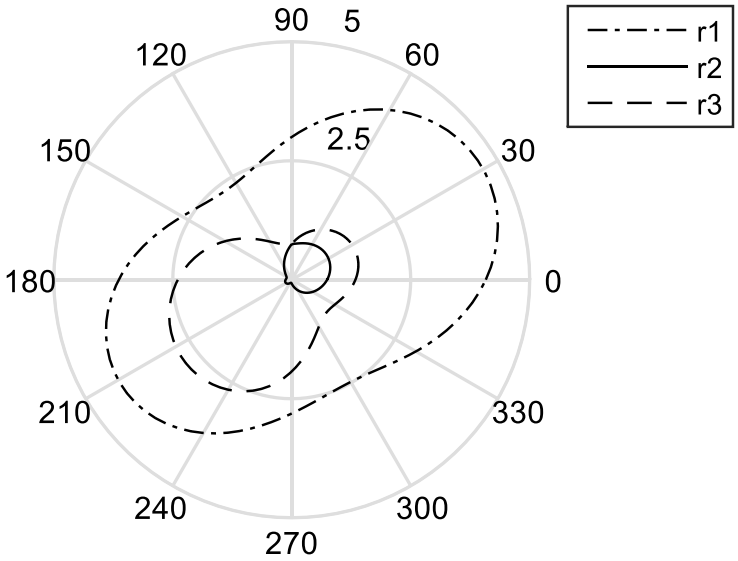

Figure 15 Mixed Mode I/II/III Tresca Invariant Form: Kr1=1, α=1, Kr2=1

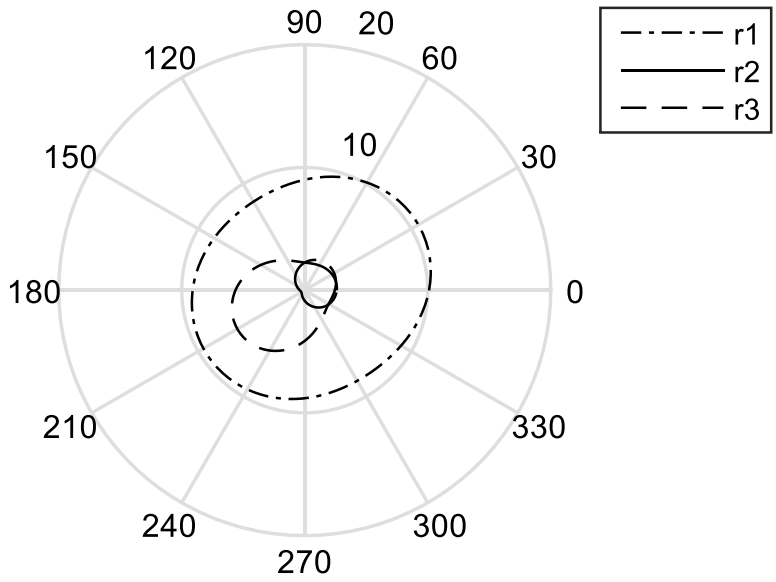

Figure 16 Mixed Mode I/II/III Tresca Invariant Form: Kr1=1, α=0.3, Kr2=2

Figures (14) through (16) show the results for the Tresca invariant form. As was the case in figures (5) through (10), r1 is always the maximum value, and thus is the only radius needed for analysis. The shape and size change patterns seen in figures (11) and (12) are present here as well for r1. However, figure (12) shows two slope discontinuities, whereas only one is present in figure (14), occurring roughly at θ=355°. This is similar to the mixed mode I/II case in the fact that no slope discontinuities were present using the Von Mises yield criterion, and then appeared in the Tresca yield criterion figures. Additionally, as mode III loading is introduced, the slope discontinuity disappears.

Tresca Principal Stress

The principal stresses are found to be:

$$\sigma_1 = \frac{1}{6}(f_{14}(1+\alpha) + \sqrt{f_{15}}\cos\left(\frac{1}{3}ArcCos\left(-\frac{f_{14}f_{16}}{f_{15}}\right)\right) \quad (79)$$

$$\sigma_2 = \frac{1}{6}(f_{14}(1+\alpha) - \sqrt{f_{15}}\cos\left(\frac{1}{3}\left(-\pi + ArcCos\left(-\frac{f_{14}f_{16}}{f_{15}}\right)\right)\right) \quad (80)$$

$$\sigma_3 = \frac{1}{6}(f_{14}(1+\alpha) - \sqrt{f_{15}}\cos\left(\frac{1}{3}\left(\pi + ArcCos\left(-\frac{f_{14}f_{16}}{f_{15}}\right)\right)\right) \quad (81)$$

where

$$f_{14} = 2\sqrt{2}\left(\cos\frac{\theta}{2} - Kr_1\sin\frac{\theta}{2}\right) \quad (82)$$

$$\begin{aligned} f_{15} = {} & 7 + 24Kr_2^2 + 16(-1+\alpha)\alpha + Kr_1^2(19 - 16\alpha + 16\alpha^2) \\ & - 4(-1 + Kr_1^2)(1-2\alpha)^2\cos\theta + 3(-1+3Kr_1^2)\cos 2\theta \\ & - 8Kr_1((1-2\alpha)^2 - 3\cos\theta)\sin\theta \end{aligned} \quad (83)$$

$$\begin{aligned} f_{16} = {} & (-1-4\alpha)\left(5 + 18Kr_2^2 + 2\alpha(-7+4\alpha)\right) + Kr_1^2\left(-41 + 2\alpha(33 + 8(3-2\alpha)\alpha)\right) \\ & + 2(27Kr_2^2 - 2(-1+2\alpha)^3 + 2Kr_1^2(-1+2\alpha)^3)\cos\theta \\ & + (-1+2\alpha)(9(-1+3Kr_1^2)\cos 2\theta \\ & + 8Kr_1((1-2\alpha)^2 + 9\cos\theta)\sin\theta) \end{aligned} \quad (84)$$

Again, using equations (22) through (24) and taking the maximum of the three, the plastic zone radius can be found. As discussed earlier, the radius is found numerically.

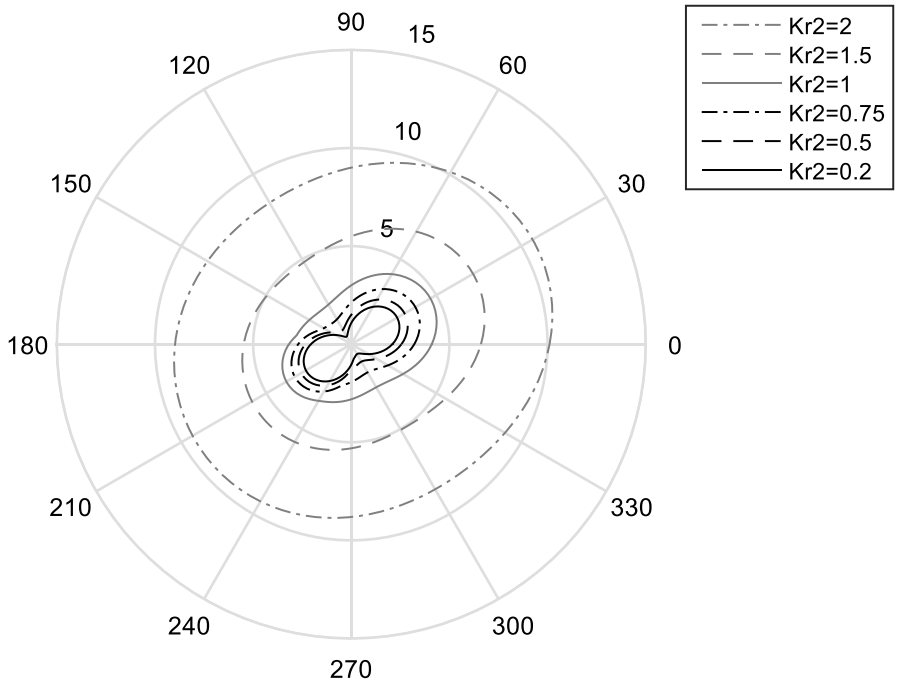

Figure 17 Mixed Mode I/II/III Tresca Principal Stress Kr1=1, α=0.3

Figure (17) matches the results seen in figures (14) through (16) as expected when using two forms of the same yield criterion. The effect of K_{III} in the form of Kr_2 can more be easily seen in figure (17) than in figures (14) through (16).

Verification

Self Verification

Several types of verification were performed on the above results to ensure their accuracy. These included self verification, comparisons to work presented in other papers at lesser complexity, and comparisons to work presented in other papers at the same level of complexity. For the self verification, it is confirmed that the results given under mode I/II/III loading conditions reduce to match those under plane strain mode I/II loading in the absence of mode III loading, and by setting α equal to ν. The former is done by setting Kr2 equal to zero. It should be noted that, as stated earlier, only the principal stresses were derived analytically for the principal stress criterion. As such, all verification of that criterion is done with respect to the principal stresses themselves, and not the radii which were generated numerically.

For the Von Mises criterion, these conditions are plugged into equation (72). This reduces to

$$r(\theta) = \frac{1}{16}(7 + 16(-1+\nu)\nu + Kr_1^2(19 + 16(-1+\nu)\nu) \\ - 4(-1 + Kr_1^2)(1-2\nu)^2\cos\theta + (-3 + 9Kr_1^2)\cos 2\theta \\ + 8Kr_1(-(1-2\nu)^2 + 3\cos\theta)\sin\theta \qquad (85)$$

which matches equation (33). For the invariant criterion, the listed conditions are combined with equations (73) through (75), and reduce to match equations (47) through (49). When reducing the results from the principal stress criterion, however, a graphical approach was required to verify the consistency of equations (79) through (81) with equations (58) through (60) under the above conditions. Figure (18) shows an exact

match. It should be noted that a value for the Poisson's ratio, when present, is required to generate graphical results. In all such cases, it is assigned a value of 0.3.

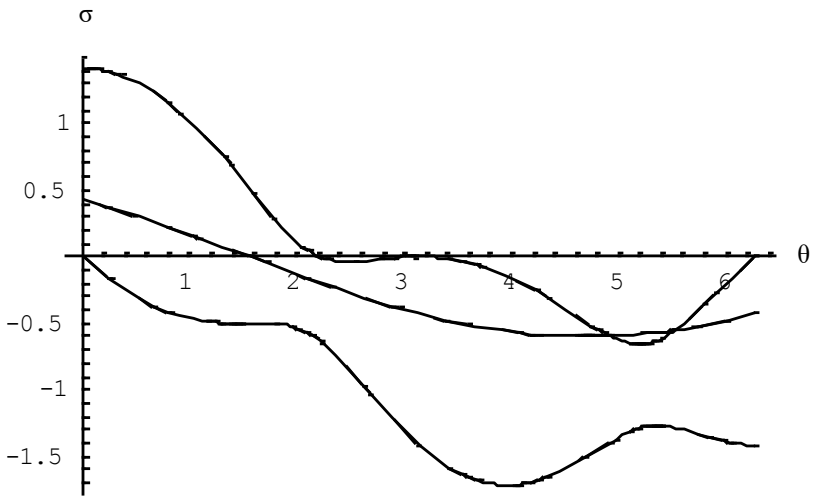

Figure 18 Comparison of Mixed Mode I/II/III to Mixed Mode I/II Principal Stress: Plane Strain

Additionally, it is confirmed that the results given using the plane strain assumption match those given using the plane stress assumption when ν is set equal to zero. For the Von Mises criterion, equation (33) reduces to

$$r(\theta) = \frac{1}{16}\left(7 + 19Kr_1^2 + (-3 + 9Kr_1^2)\cos 2\theta - 8Kr_1 \sin\theta + 4\cos\theta\,(1 - Kr_1^2 + 6Kr_1 \sin\theta)\right) \quad (86)$$

which matches equation (32). For the invariant criterion, equations (47) through (49) reduce to match equations (42) through (44). Similarly, for the principal stress criterion, equations (58) through (60) reduce to match (52) through (54).

Single Mode Loading Verification

Much work has been presented for the plastic zone size under an individual loading mode, so it is important to confirm the work presented in this paper can reduce to these simpler cases. Results present by Jing et al. (2003, 2004) are used for comparisons, as those papers use all three yield criteria used in this paper, whereas all other papers

found by this author only present work using the Von Mises yield criterion. For mode III loading, the comparison is made with the reduced results of the mode I/II/III loading work. For mode I loading and mode II loading, the comparisons are made with the reduced results from the mode I/II loading work.

To verify the pure mode I loading case, Kr1 is set to zero. Using the Von Mises criterion, equations (32) and (33) reduce to

$$r = \frac{1}{16}[7 + 4\cos(\theta) - 3\cos(2\theta)] \qquad (87)$$

for plane stress, and

$$r = \frac{1}{4}(\cos^2(\theta))[5 - 8\nu + 8\nu^2 - 3\cos(\theta)] \qquad (88)$$

for plane strain, which match equations (30) and (38), respectively, from Jing et al. (2004). For both the invariant and principal stress criteria, a graphical verification was required. Figures (19) through (22) below show exact matches for each criterion, under both plane stress and plane strain, with the results from Jing et al. (2004).

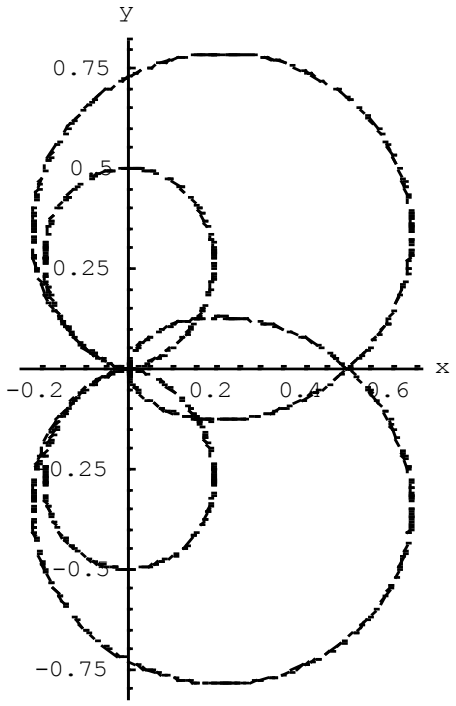

Figure 19 Pure Mode I Tresca Invariant Form: Plane Stress

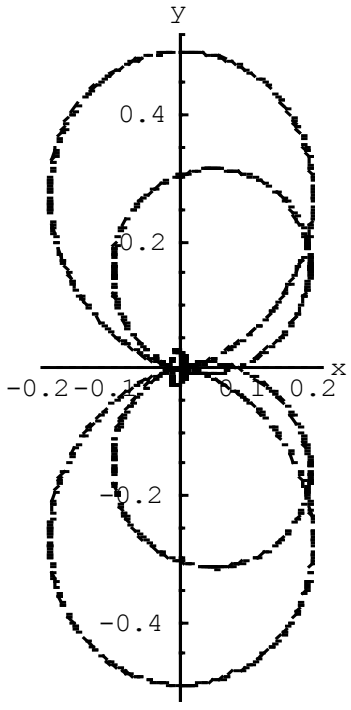

Figure 20 Pure Mode I Tresca Invariant Form: Plane Strain, v=0.3

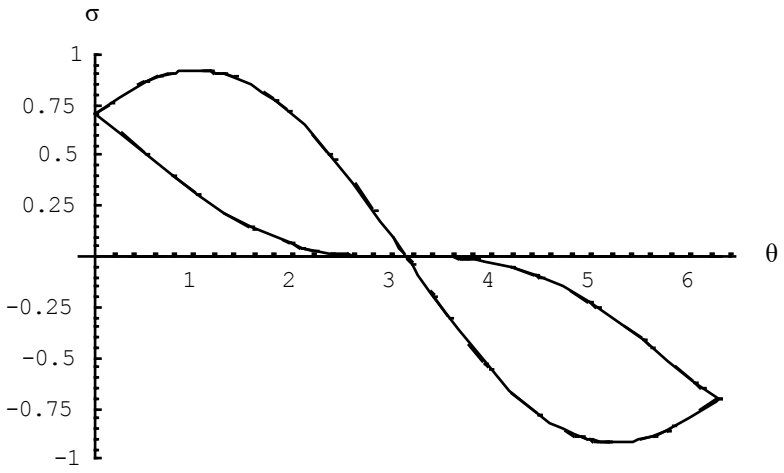

Figure 21 Pure Mode I Tresca Principal Stresses: Plane Stress

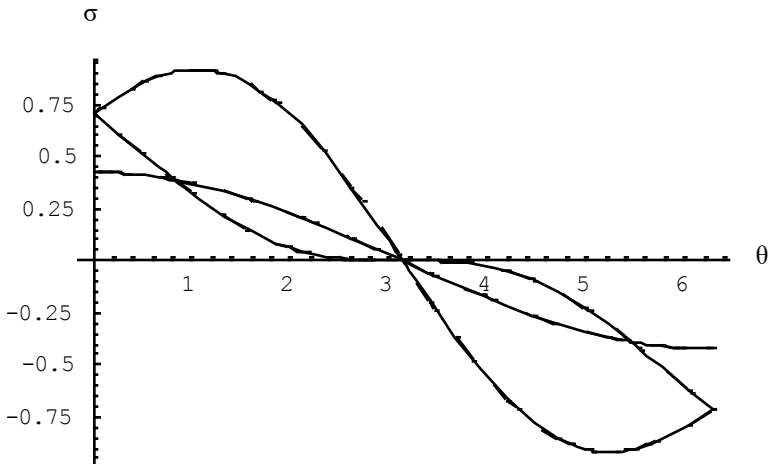

Figure 22 Pure Mode I Tresca Principal Stresses: Plane Strain, v=0.3

Verification for the pure mode II and pure mode III cases are not as simple. All original work presented in this paper is normalized with respect to K_I, but in the absence of mode I loading, it is necessary to normalize with respect to a different stress intensity factor. Specifically, the results need to be normalized with respect to the single mode present, K_{II} for mode II loading and K_{III} for mode III loading. The remaining loading

modes must then be removed by setting their respective stress intensity factor to zero. However, the results must first be de-normalized with respect to K_I due to its presence in the denominator of the normalized radii and principal stresses. This is done simply by multiplying the expressions for the plastic zone radius or principal stresses by K_I of the appropriate order. For the Von Mises and Tresca invariant criteria, this entails multiplying by K_I^2. For the Tresca principal stress criterion, the results are multiplied by K_I. Next, the stress intensity factor ratio variables must be replaced with the actual K terms, i.e. Kr_1 is replaced with K_{II}/K_I and Kr_2 is replaced with K_{III}/K_I. Some additional algebraic manipulation is done to simplify the expressions.

Results from the mixed mode I/II loading case are used as the starting point for the pure mode II loading verification. After the above steps are performed, K_I is set to zero, and K_{II}, of the appropriate order described above, is divide through to re-normalize the result. For the Von Mises yield criterion, this gives

$$r = \frac{1}{16}(19 - 4\cos(\theta) + 9\cos(2\theta)) \qquad (89)$$

for plane stress, and

$$r = \frac{1}{16}(19 + 16(-1 + \nu)\nu - 4(1 - 2\nu)^2\cos(\theta) + 9\cos(2\theta)) \qquad (90)$$

for plane strain. These match equations (12) and (19) from Jing et al. (2003), respectively. As was the case for pure mode I loading, both Tresca yield criteria for pure mode II loading required graphical verification. Figures (23) through (26) below show the required consistency between the work presented in this paper and the work presented by Jing et al. (2003).

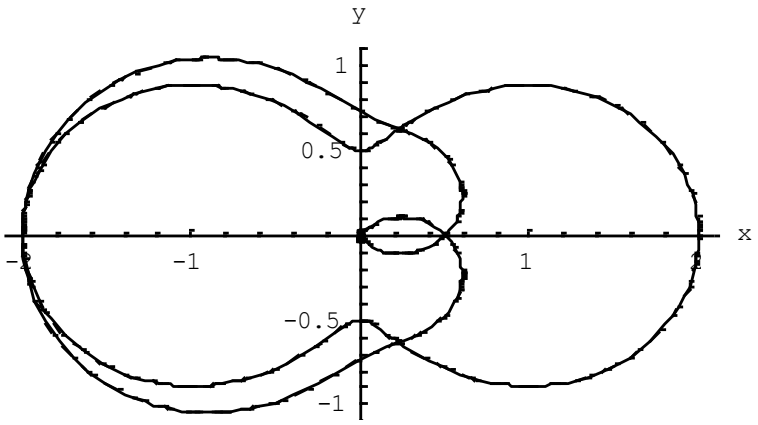

Figure 23 Pure Mode IITresca Invariant Form: Plane Stress

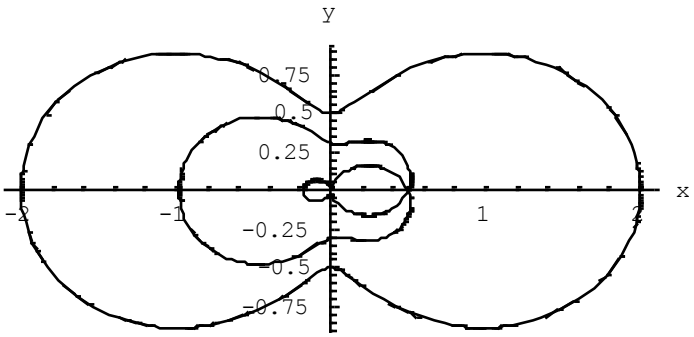

Figure 24 Pure Mode II Tresca Invariant Form: Plane Strain, v=0.3

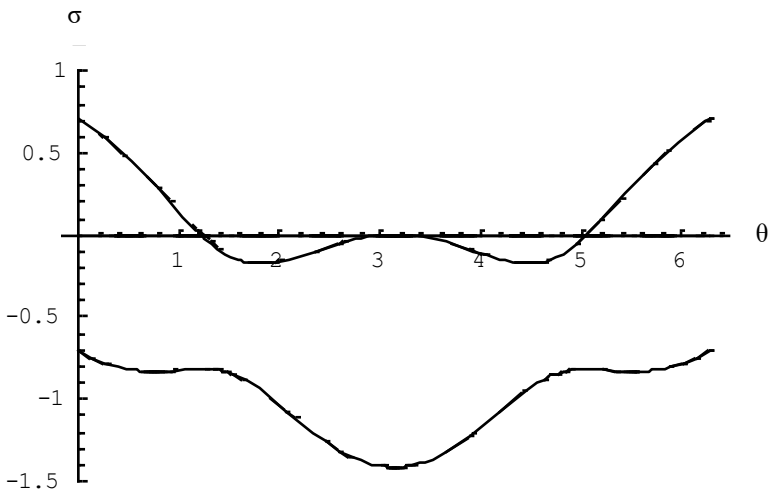

Figure 25 Pure Mode II Tresca Principal Stress: Plane Stress

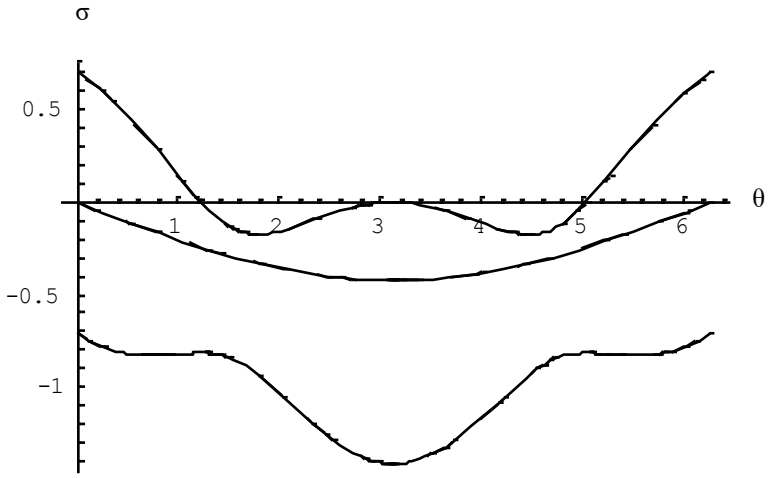

Figure 26 Pure Mode II Tresca Principal Stress: Plane Strain, v0.3

The same process used for pure mode II verification is used for pure mode III, except the results start from the mixed mode I/II/III loading case, are re-normalized with respect to K_{III}, and K_{II} is also set to zero. Additionally, Jing et al. (2004) does not include

results for the Tresca principal stress criterion, so no verification could be made. After simplification, the radius found using the Von Mises criterion reduces to

$$r = 1.5 \quad (91)$$

matching equation (51) from Jing et al. (20004). The Tresca invariant form criterion gives

$$r_2 = r_3 = 0.5 \quad (92)$$

and

$$r_1 = 2 \quad (93)$$

The only discrepancy between equations (92) and (93) here and equations (52) and (53) in Jing et al. (2004) is that r_1 and r_3 are swapped, but this is not a meaningful difference.

Mixed Mode Loading Verification

The final set of verification tests compared results for mixed mode I/II from the presented work with results obtained from Khan and Khraisheh (2004) and Golos and Wasiluk (2000). It should be noted that both papers only consider the Von Mises yield criterion, and thus no verifications involving either Tresca yield criteria can be made. Golos and Wasiluk presented a solution for the plane stress case, written in equation (27) in that paper and shown below as equation (94). Normalization and some algebraic manipulation are required to compare to the results found in this paper.

$$R = \frac{1}{2\pi\sigma_{ys}^2}\left[K_I^2\cos^2\left(\frac{\theta}{2}\right)\left(1+3\sin^2\left(\frac{\theta}{2}\right)\right) + K_I K_{II}\sin(\theta)\left(3\cos(\theta)-1\right)\right.$$
$$\left. + K_{II}^2\left\{3+\sin^2\left(\frac{\theta}{2}\right)\left(1-9\cos^2\left(\frac{\theta}{2}\right)\right)\right\}\right] \quad (94)$$

To normalize equation (94), the radius is multiplied by $2\pi\sigma_{ys}^2/K_I^2$. After substituting in Kr1 for K_{II}/K_I and a little simplification, equation (94) becomes

$$r(\theta) = \frac{1}{16}\big(7 + 19Kr_1^2 + (-3 + 9Kr_1^2)\cos 2\theta - 8Kr_1 \sin\theta + 4\cos\theta\,(1 - Kr_1^2 + 6Kr_1 \sin\theta)\big) \qquad (95)$$

which matches equation (32).

Khan and Khraisheh present solutions for both the plane stress and plane strain conditions. It should be noted that these results are normalized with respect to terms common between K_I and K_{II}. However, performing another normalization with respect to the remaining part of K_I can be done to match the presented work. Additionally, Khan and Khraisheh use an angled crack, measured clockwise from the Y-axis. This angle is set to 90° for comparison. Performing the above on equations (24a) and (24b) from Khan and Khraisheh (2004) gives

$$r(\theta) = \frac{1}{16}\big(7 + 19Kr_1^2 + (-3 + 9Kr_1^2)\cos 2\theta - 8Kr_1 \sin\theta + 4\cos\theta\,(1 - Kr_1^2 + 6Kr_1 \sin\theta)\big) \qquad (96)$$

for plane stress and

$$r(\theta) = \frac{1}{16}(7 + 16(-1 + \nu)\nu + Kr_1^2(19 + 16(-1 + \nu)\nu) - 4(-1 + Kr_1^2)(1 - 2\nu)^2\cos\theta + (-3 + 9Kr_1^2)\cos 2\theta + 8Kr_1(-(1 - 2\nu)^2 + 3\cos\theta)\sin\theta \qquad (97)$$

for plane strain, which match equations (32) and (33) respectively. It should be noted that a coordinate transformation matrix could be applied to the presented work to obtain the more general crack alignment seen in Khan and Khraisheh.

Other Mixed Modes

Results for both mixed mode I/II and mixed mode I/II/III were directly solved for, but results for mixed mode I/III and mixed mode II/III can be derived from the mixed mode I/II/III case. The same general behavioral pattern seen above is also present in the results for mixed mode I/III (figures (27) through (31)), and mixed mode II/III (figures (32) through (36)). Higher values for Kr_2 and Kr_4 (see equation 111), those with K_{III} in the numerator, have fairly circular radii as K_{III} is more dominant. Additionally, these higher ratios lead to larger radii. As the respective K ratio decreases, the radii move closer to those of pure mode I or pure mode II loading.

Mixed Mode I/III

To find solutions for mixed mode I/III, the only step needed is to set K_{II} equal to zero, which makes Kr_1 equal to zero as well. For the Von Mises yield criterion, this gives

$$r = \frac{1}{16}(7 + 24Kr_2^2 + 16(-1+\alpha)\alpha + 4(1-2\alpha)^2\cos(\theta) - 3\cos(2\theta)) \qquad (98)$$

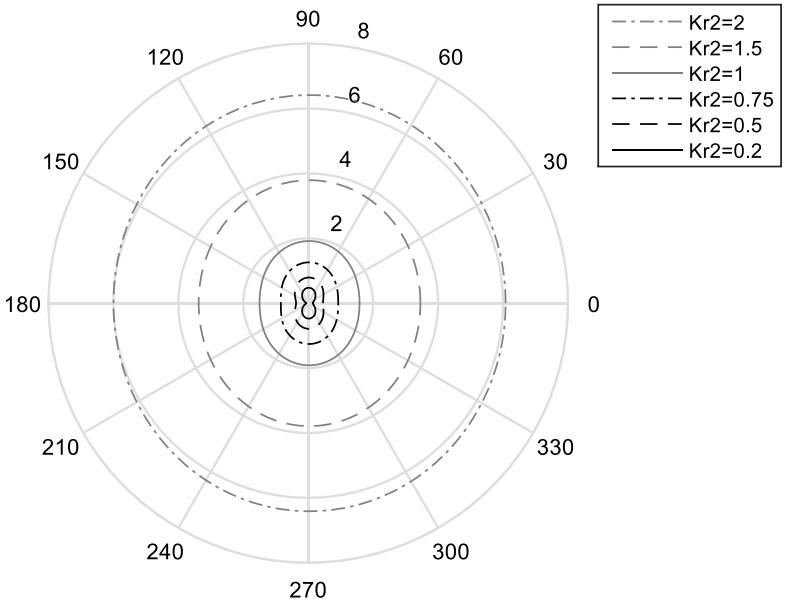

Figure 27 Mixed Mode I/III Von Mises: α=0.3

For the Tresca Invariant form criterion, this gives

$$r_1 = \frac{1}{24} f_{17} \left(1 + \cos\left(\frac{1}{3}\text{ArcCos}\left(\frac{-f_{17}^3 + 2(f_{17}^3 - f_{18})}{f_{17}^3}\right)\right)\right) \qquad (99)$$

$$r_2 = \frac{1}{24} f_{17} \left(1 - \cos\left(\frac{1}{3}\left(-\pi + \text{ArcCos}\left(\frac{-f_{17}^3 + 2(f_{17}^3 - f_{18})}{f_{17}^3}\right)\right)\right)\right) \qquad (100)$$

$$r_3 = \frac{1}{24} f_{17} \left(1 - \cos\left(\frac{1}{3}\left(\pi + \text{ArcCos}\left(\frac{-f_{17}^3 + 2(f_{17}^3 - f_{18})}{f_{17}^3}\right)\right)\right)\right) \qquad (101)$$

where

$$f_{17} = 7 + 24Kr_2^2 + 16(-1+\alpha)\alpha + 4(1-2\alpha)^2\cos(\theta) - 3\cos(2\theta) \qquad (102)$$

and

$$f_{18} = 8\cos^2\left(\frac{\theta}{2}\right)\Big((-1-4\alpha)\big(5 + 18Kr_2^2 + 2\alpha(-7+4\alpha)\big) + 2(27Kr_2^2 - 2(-1+2\alpha)^3)\cos(\theta) - 9(-1+2\alpha)\cos(2\theta)\Big)^2 \qquad (103)$$

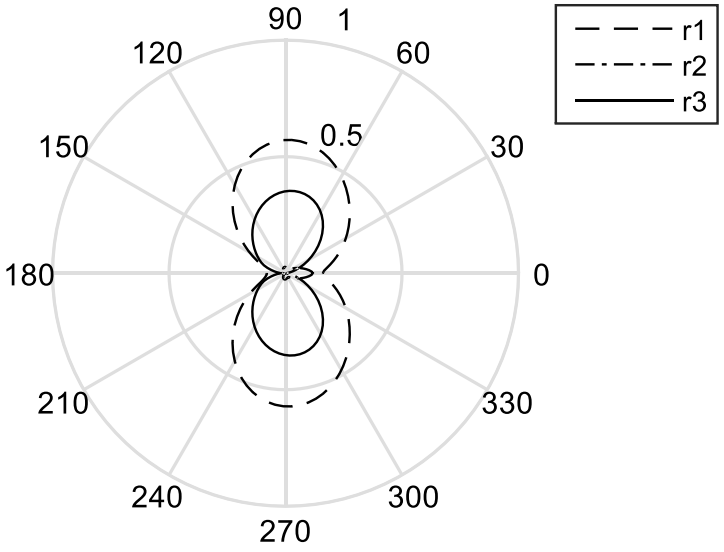

Figure 28 Mixed Mode I/III Tresca Invariant Form: α=0.3, Kr2=0.2

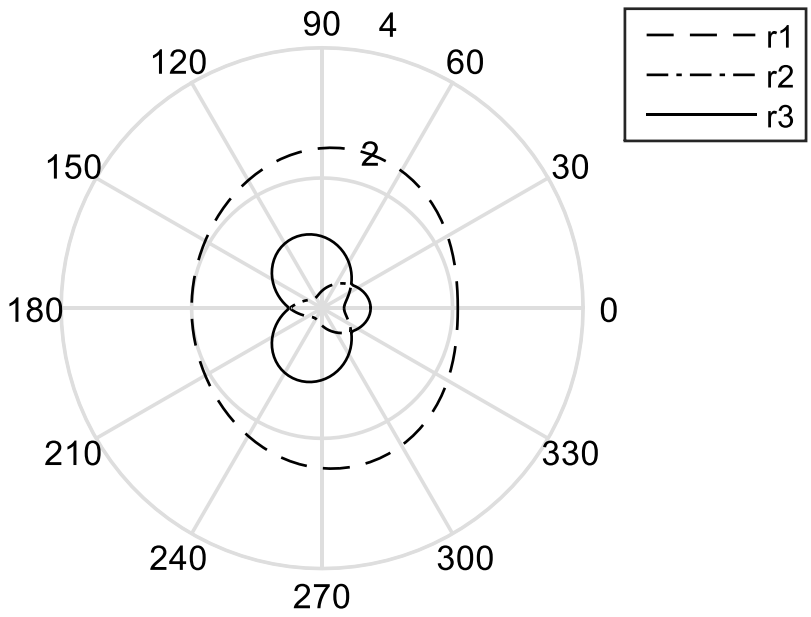

Figure 29 Mixed Mode I/III Tresca Invariant Form: α=0.3, Kr2=1

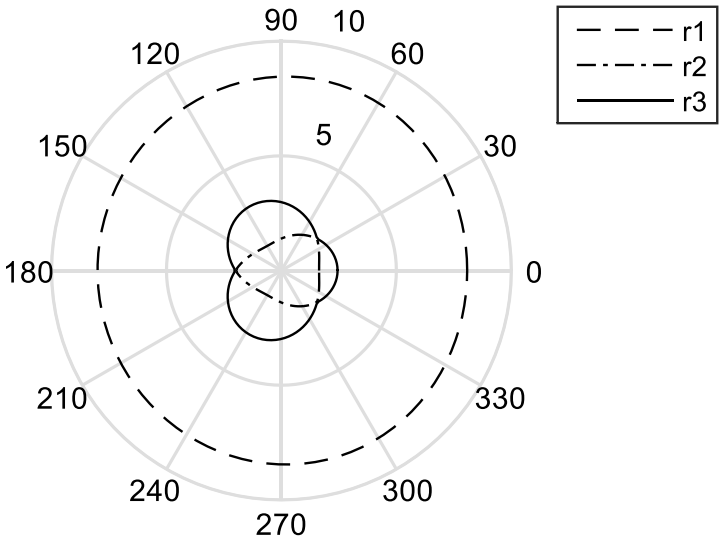

Figure 30 Mixed Mode I/III Tresca Invariant Form: α=0.3, Kr2=2

The Tresca principal stress criterion gives

$$\sigma_1 = \frac{1}{6}\left(f_{21} + \sqrt{f_{19}}\cos\left(\frac{1}{3}\text{ArcCos}\left(\frac{f_{21}f_{20}}{\sqrt{f_{19}^3}}\right)\right)\right) \qquad (104)$$

$$\sigma_2 = \frac{1}{6}\left(f_{21} - \sqrt{f_{19}}\cos\left(\frac{1}{3}\left(-\pi + \text{ArcCos}\left(\frac{f_{21}f_{20}}{\sqrt{f_{19}^3}}\right)\right)\right)\right) \qquad (105)$$

$$\sigma_3 = \frac{1}{6}\left(f_{21} - \sqrt{f_{19}}\cos\left(\frac{1}{3}\left(\pi + \text{ArcCos}\left(\frac{f_{21}f_{20}}{\sqrt{f_{19}^3}}\right)\right)\right)\right) \qquad (106)$$

where

$$f_{19} = 7 + 24Kr_2^2 + 16(-1+\alpha)\alpha + 4(1-2\alpha)^2\cos(\theta) - 3\cos(2\theta) \qquad (107)$$

$$f_{20} = (1+4\alpha)(5 + 18Kr_2^2 - 14\alpha + 8\alpha^2) + (-54Kr_2^2 + 4(-1+2\alpha)^3)\cos(\theta) + 9(-1+2\alpha)\cos(2\theta) \qquad (108)$$

and

$$f_{21} = 2\sqrt{2}\cos\left(\frac{\theta}{2}\right)(1+\alpha) \qquad (109)$$

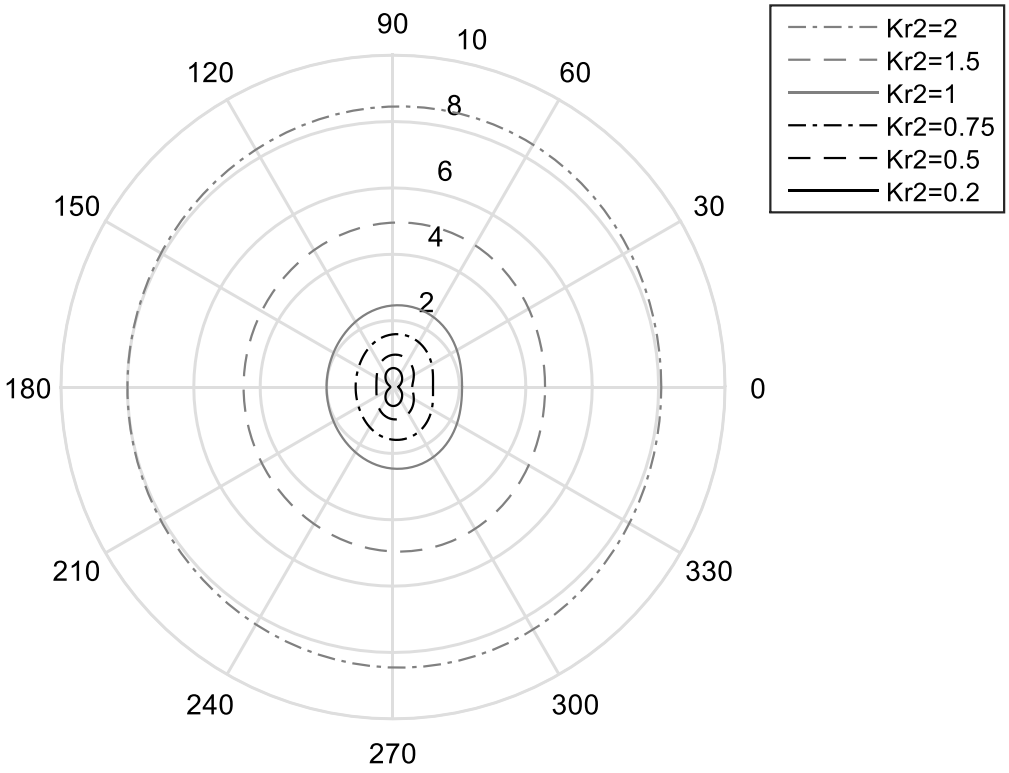

Figure 31 Mixed Mode I/III Tresca Principal Stress: α=0.3

Mixed Mode II/III

Mixed mode II/III requires a more algebraic manipulation. Similar to what was shown when verifying the presented work will reduce to pure mode II or pure mode III loading, the results for mixed mode I/II/III loading must be de-normalized with respect to K_I. Following this, the results can be normalized with respect to K_{II}, and two new stress intensity factor ratios are created.

$$Kr_3 = \frac{K_I}{K_{II}} \qquad (110)$$

$$Kr_4 = \frac{K_{III}}{K_{II}} \qquad (111)$$

Finally, K_I is set to zero, making Kr_3 equal to zero. For the Von Mises criterion, this gives

$$r = \frac{1}{16}(19 + 24Kr_4^3 + 16(-1+\alpha)\alpha - 4(1-2\alpha)^2\cos(\theta) + 9\cos(2\theta)) \qquad (112)$$

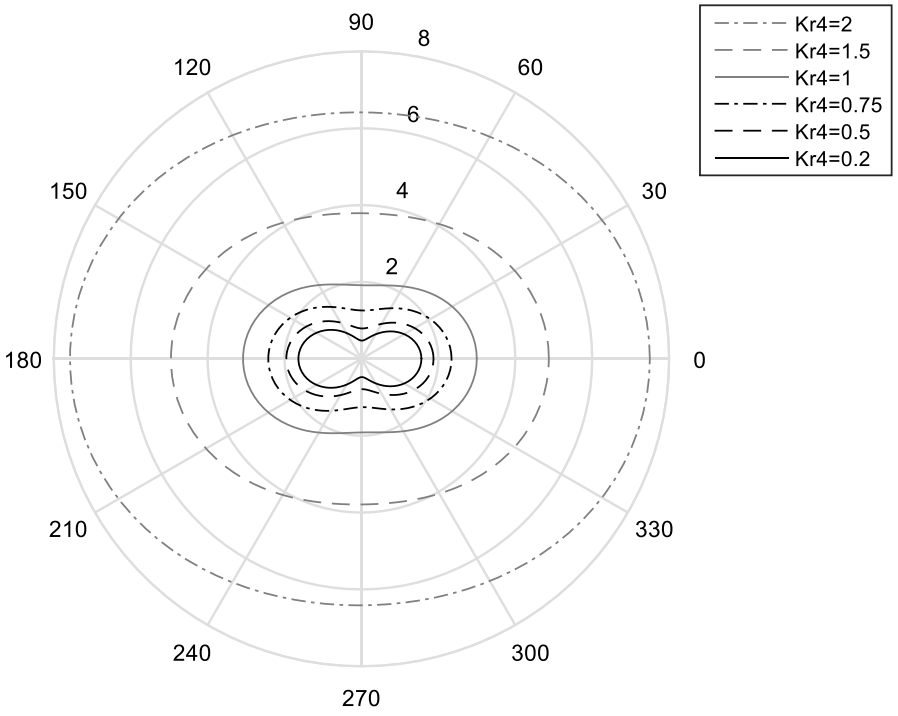

Figure 32 Mixed Mode II/III Von Mises: α=0.3

For the Tresca invariant form this gives

$$r_1 = \frac{1}{24} f_{22}\left(1 + \cos\left(\frac{1}{3} ArcCos\left(\frac{-f_{22}^3 + 2(f_{22}^3 - f_{23})}{f_{22}^3}\right)\right)\right) \qquad (113)$$

$$r_2 = \frac{1}{24} f_{22}\left(1 - \cos\left(\frac{1}{3}\left(-\pi + ArcCos\left(\frac{-f_{22}^3 + 2(f_{22}^3 - f_{23})}{f_{22}^3}\right)\right)\right)\right) \qquad (114)$$

$$r_3 = \frac{1}{24} f_{22}\left(1 - \cos\left(\frac{1}{3}\left(\pi + ArcCos\left(\frac{-f_{22}^3 + 2(f_{22}^3 - f_{23})}{f_{22}^3}\right)\right)\right)\right) \qquad (115)$$

where

$$f_{22} = 19 + 24Kr_4^3 + 16(-1+\alpha)\alpha - 4(1-2\alpha)^2\cos(\theta) + 9\cos(2\theta) \qquad (116)$$

and

$$f_{23} = 8\sin^2\left(\frac{\theta}{2}\right)(-41 - 18Kr_4^3(1+4\alpha) + 2\alpha(33 + 8(3-2\alpha)\alpha) + 2(27Kr_4^2 + 2(-1+2\alpha)^3)\cos(\theta) + 27(-1+2\alpha)\cos(2\theta))^2 \qquad (117)$$

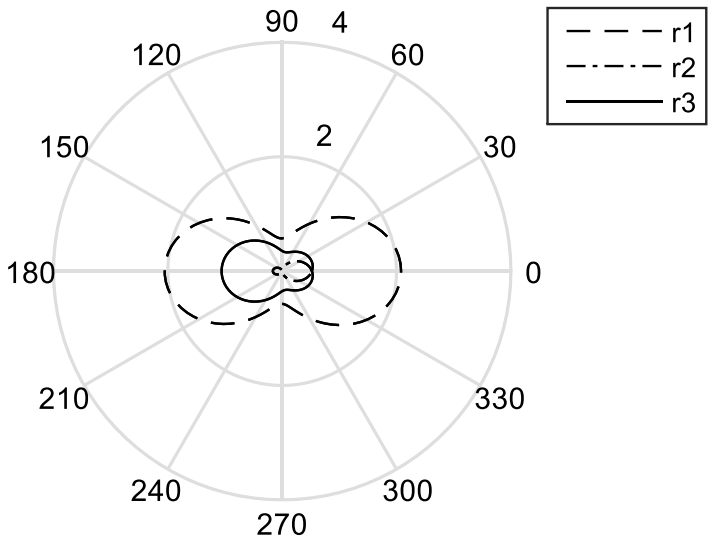

Figure 33 Mixed Mode II/III Tresca Invariant Form: α=0.3, Kr4=0.2

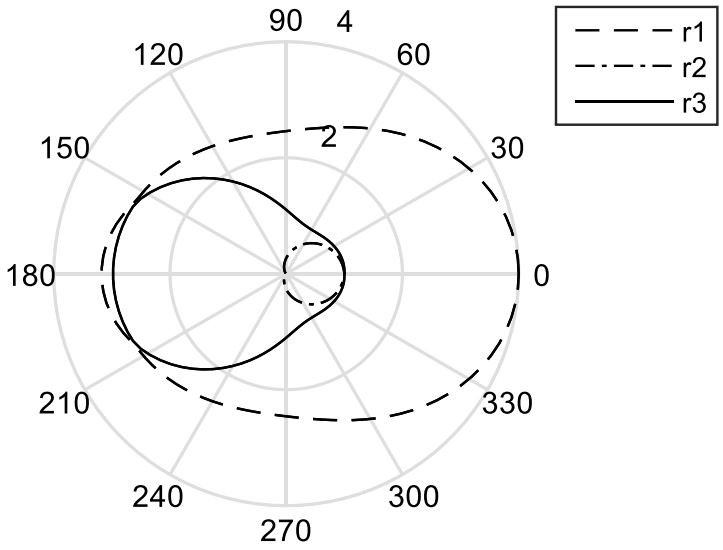

Figure 34 Mixed Mode II/III Tresca Invariant Form: α=0.3, Kr4=1

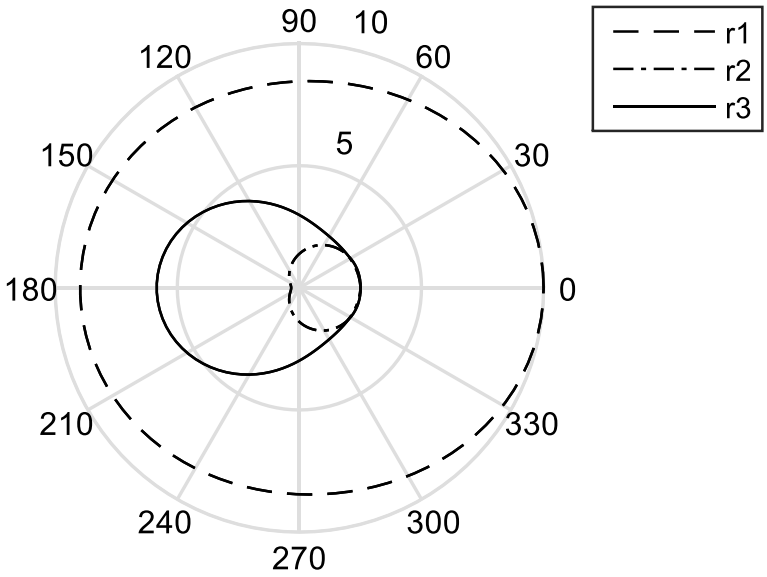

Figure 35 Mixed Mode II/III Tresca Invariant Form: α=0.3, Kr4=2

Finally, the Tresca principal stress criterion gives

$$\sigma_1 = \frac{1}{6}\left(\sqrt{f_{24}}\cos\left(\frac{1}{3}ArcCos\left(\frac{f_{25}f_{26}}{\sqrt{f_{24}^3}}\right)\right) - f_{26}(1+\alpha)\right) \qquad (118)$$

$$\sigma_2 = \frac{1}{6}\left(\sqrt{f_{24}}\cos\left(\frac{1}{3}\left(-\pi + ArcCos\left(\frac{f_{25}f_{26}}{\sqrt{f_{24}^3}}\right)\right)\right) - f_{26}(1+\alpha)\right) \qquad (119)$$

$$\sigma_3 = \frac{1}{6}\left(\sqrt{f_{24}}\cos\left(\frac{1}{3}\left(\pi + ArcCos\left(\frac{f_{25}f_{26}}{\sqrt{f_{24}^3}}\right)\right)\right) - f_{26}(1+\alpha)\right) \qquad (120)$$

where

$$f_{24} = 19 + 24Kr_4^3 + 16(-1+\alpha)\alpha - 4(1-2\alpha)^2\cos(\theta) + 9\cos(2\theta) \qquad (121)$$

$$f_{25} = \quad -41 - 18Kr_4^2(1+4\alpha) + 2\alpha(33 + 8(3-2\alpha)\alpha) + 2(27Kr_4^2 + 2(-1+2\alpha)^3)\cos(\theta)) \qquad (122)$$

and

$$f_{26} = 2\sqrt{2}\sin\left(\frac{\theta}{2}\right) \qquad (123)$$

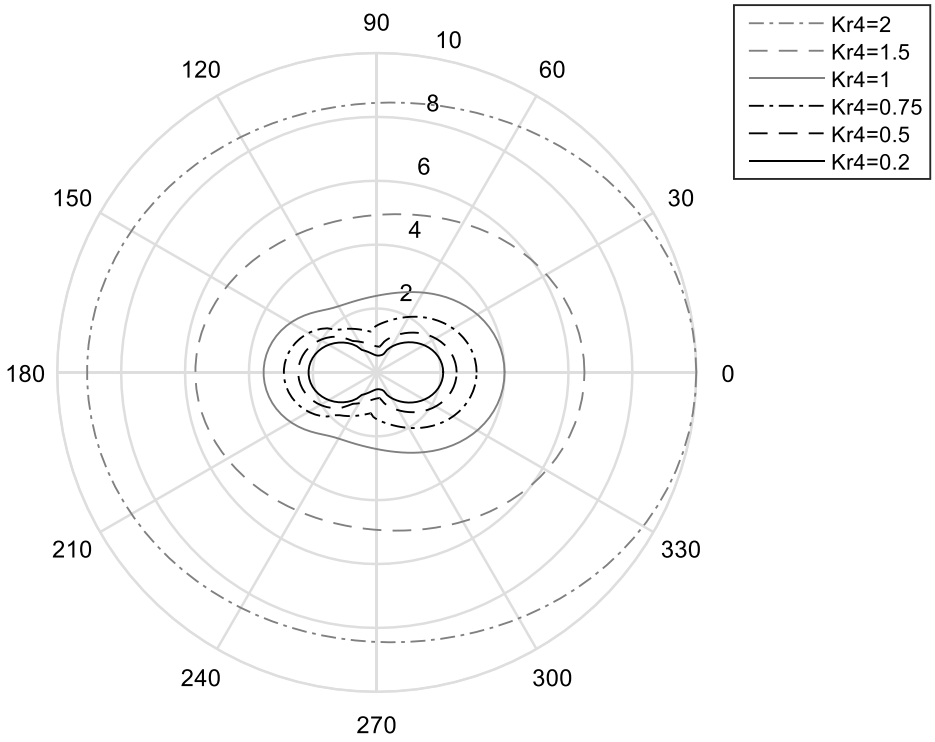

Figure 36 Mixed Mode II/III Tresca Principal Stress: α=0.3

Results

Area Analysis

One technique for evaluating the difference in results given by the Von Mises and Tresca yield criteria is an area analysis. By simply overlaying the plastic zone figures, a comparison can be made. Figure (37) shows the radii for each under mixed mode I/II loading, using the plane stress assumption. Figure (38) shows the radii under mixed mode I/II/III loading. It can be seen in each figure that the plastic zone area using the Tresca criterion is larger than that of the Von Mises criterion. The Tresca yield criterion is generally considered a more conservative yield criterion, meaning it is expected that it would predict a larger plastically deformed area than would be predicted using the Von Mises yield criterion.

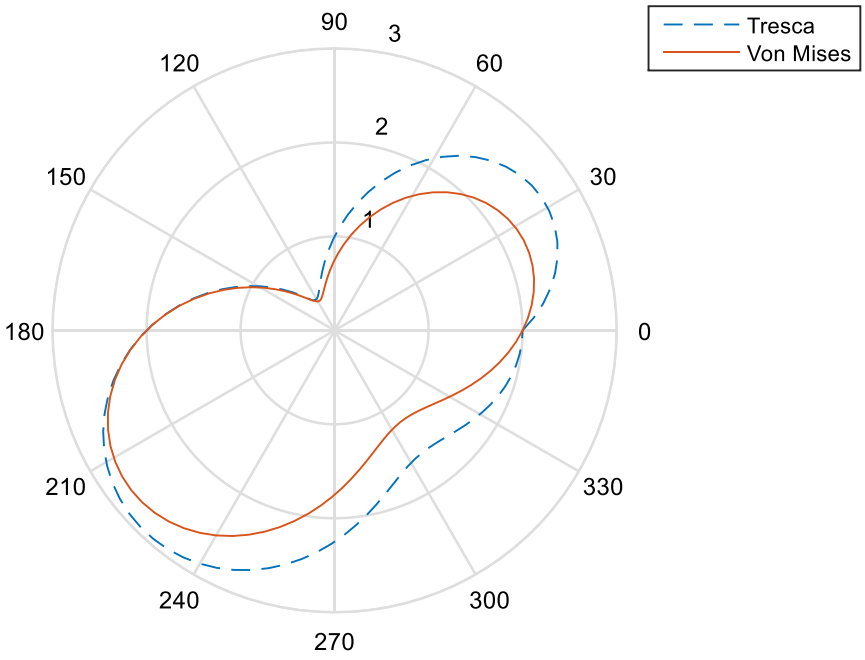

Figure 37 Area comparison under mixed mode I/II loading: Plane Stress, Kr1=1

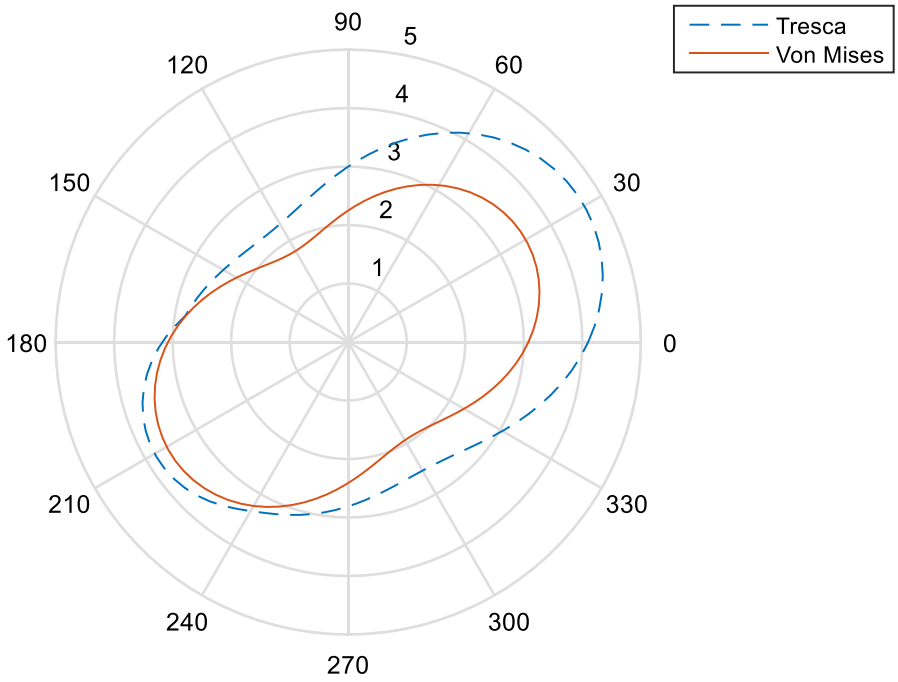

Figure 38 Area comparison under mixed mode I/II/III loading: Kr1=1, α=0.3, Kr2=1

Crack Propagation

In addition to determining the plastic zone radius, it is also important to determine the angle at which the crack will grow. There are several existing criteria, including the maximum tangential stress criterion (Erdogan and Sih, 1963), and the Y-criterion (Yehia, 1991). The criterion investigated here is the R-criterion, presented by Khan and Khraisheh (2004). As mentioned earlier, they theorized that the crack will grow through the plastic zone, a region of highly strained material, following the "easiest" path. They assume this easiest path is the shortest distance between the crack-tip and the elastic region, the shortest distance referring to the minimum radius of the plastic zone. Additionally, it was stated that this minimum radius represents the minimum plastic work needed to create cracked surfaces. The R-criterion is defined mathematically as:

$$\frac{\partial R}{\partial \theta} = 0 \qquad \frac{\partial^2 R}{\partial \theta^2} > 0 \qquad (124)$$

This paper seeks to find if any correlation exists between the principal stresses and the minimum plastic zone radius as it applies to the crack initiation angle. The mixed-mode I/II loading case, under the plane stress assumption, is used for comparison. First, the minimum radius of the plastic zone from the work presented earlier is found. An exact angle is not required, so Matlab is used to find an approximate value for the θ at which the minimum radius occurs. Mathematically, the two extremes of this angle occur in the presence of either pure mode I loading, or pure mode II loading. Pure mode I loading will give an angle of zero. Pure mode II loading will give an angle of -82.5, where a positive angle is measured counterclockwise from the x-axis. This means the minimum radius will occur at an angle between these two extremes. This angle is found for a range of Kr_I values, and is compared the principal stress direction found using Mohr's circle. However, since this direction does not correspond to a specific principal stress, both principal stress directions are found using the eigenvalue problem method in order to determine which may have a correlation. The formulas to find these directions, as well as the principal stresses from Mohr's circle, are shown in the appendix. A principal shear direction is also shown, and can be found by subtracting 45° from a principal stress direction.

$$\theta = \frac{1}{2}\tan^{-1}\left(\frac{2\sigma_{xy}}{\sigma_{xx} - \sigma_{yy}}\right) \qquad (125)$$

Figure (39) shows the resulting plots. It can be seen that the principal stress direction obtained from Mohr's circle, shown in equation (125), corresponds to the 2nd principal stress for all Kr_I values. More importantly, the figure shows that the angle at

which the minimum radius occurs will match the principal stress direction of the 2nd principal stress only under pure mode I loading, i.e. Kr_I=0. As mode II loading is introduced and becomes more and more prevalent, the angle of the minimum radius deviates from the principal stress direction toward a principal shear direction, although never becoming equal. However, this does not mean the principal stresses have no effect on the minimum radius location. The fact that it moves clockwise as Kr_I increases is a direct result of the principal stresses present due to the type of loading.

Additionally, figure (39) contains data experimentally collected by Erdogan and Sih (1963) and Theocaris et al. (1982). The results were crack initiation angles obtained by pulling a plate in tension. The experiments were performed with an angled crack, creating mixed-mode loading local to the crack-tip. This implies a direct relation between the crack inclination angle, β, and the stress intensity factor ratio, Kr_I. Equation (126) shows this relation. The derivation can be seen in the appendix.

$$Kr_1 = Tan\left(\frac{\pi}{2} - \beta\right) \quad (126)$$

It can be seen that for small Kr_I values, the minimum radius matches well with the experimental data. However, as Kr_I grows beyond 1, the experimental data starts to deviate. This is likely due to an imperfect experimental setup. Instead of having pure mode II loading, as should happened as $Kr_I \rightarrow \infty$, a vertical crack will have no applied tearing mode at all under the same tensile load.

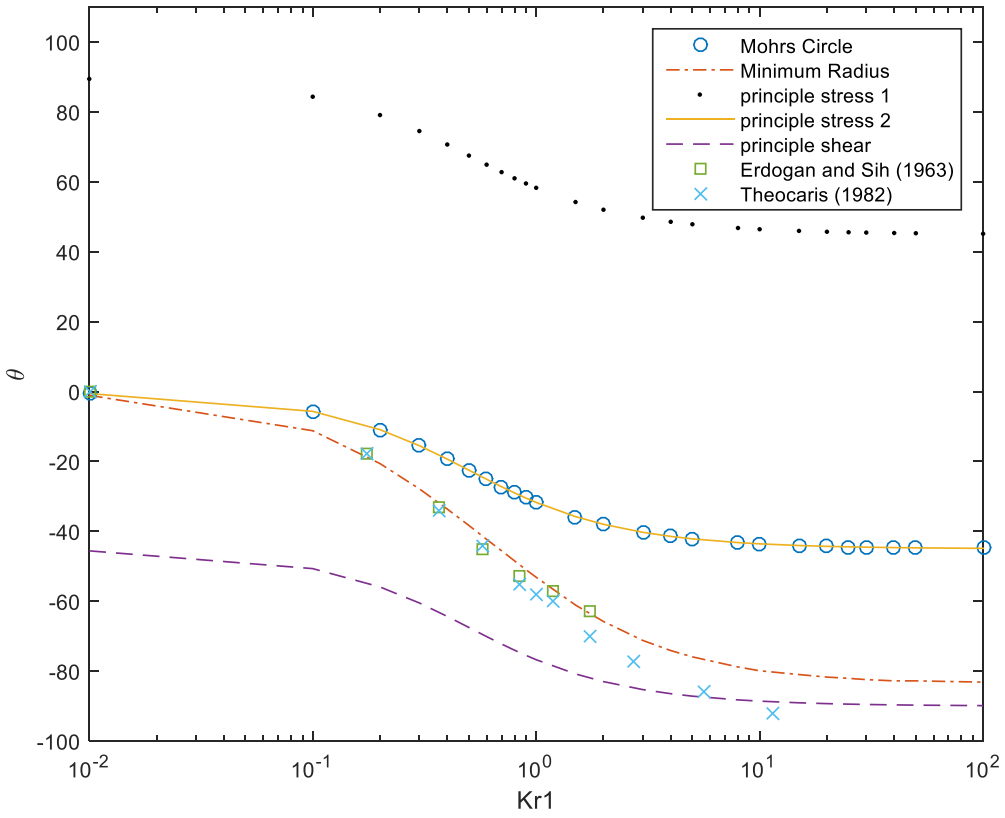

Figure 39 Minimum Radius Vs. Principal Stress and Shear Directions

Conclusions

Analytic solutions for the plastic zone radius were found for mixed mode I/II, mixed mode I/II/III, mixed mode I/III, and mixed mode II/III loading using the Von Mises, Tresca invariant form, and Tresca principal stress criteria. Each was verified to reduce to the individual loading modes separately. It was shown that as an individual stress intensity factor ratio grows larger, a single loading mode becomes dominant, i.e. mode II when Kr1 becomes large, and the results shift closer and closer to those given under pure loading of that mode. It can be seen that as the Poisson's ratio increases, the plastic zone size decreases. The Tresca yield criterion displayed larger plastic zone areas than the Von Mises yield criterion. It was shown that, except in the case of pure mode I

loading, the crack initiation angle predicted by the R-criterion does not occur at a principal stress or principal shear direction. However, the principal stresses do play an important role in the location of the minimum plastic zone radius used by the R-criterion.

Appendix

Principal stresses from Mohr's circle:

$$\sigma_1 = \frac{\sigma_{xx} + \sigma_{yy}}{2} + \sqrt{\frac{1}{4}(\sigma_{xx} - \sigma_{yy})^2 + \sigma_{xy}^2}$$

$$\sigma_2 = \frac{\sigma_{xx} + \sigma_{yy}}{2} - \sqrt{\frac{1}{4}(\sigma_{xx} - \sigma_{yy})^2 + \sigma_{xy}^2}$$

Principal stress direction:

$$\theta = \frac{1}{2}\tan^{-1}\left(\frac{2\sigma_{xy}}{\sigma_{xx} - \sigma_{yy}}\right) = \frac{1}{2}\tan^{-1}\left(\frac{2\sigma_{xy}}{-\sigma_{yy}}\right) = \frac{1}{2}\tan^{-1}\left(\frac{-2K_{II}}{K_I}\right) = \frac{1}{2}\tan^{-1}(-2Kr_1)$$

$$\begin{bmatrix} \sigma_{xx} - \sigma & \sigma_{xy} & \sigma_{xz} \\ \sigma_{xy} & \sigma_{yy} - \sigma & \sigma_{yz} \\ \sigma_{xz} & \sigma_{yz} & \sigma_{zz} - \sigma \end{bmatrix} \begin{Bmatrix} l \\ m \\ n \end{Bmatrix} = \begin{Bmatrix} 0 \\ 0 \\ 0 \end{Bmatrix}$$

For mixed-mode I/II using far-field stresses:

$$\sigma_{xx} = \sigma_{xz} = \sigma_{yz} = \sigma_{zz} = 0 \quad and\ n = 0$$

$$-\sigma l + \sigma_{xy} = 0 \quad \rightarrow \quad l = \frac{\sigma_{xy}}{\sigma} m$$

$$l^2 + m^2 = 1 \quad \rightarrow \quad m^2 = 1 - l^2 = 1 - \left(\frac{\sigma_{xy}}{\sigma} m\right)^2$$

$$m^2\left(1 + \left(\frac{\sigma_{xy}}{\sigma}\right)^2\right) = 1 \quad \rightarrow \quad m = \pm\sqrt{\frac{1}{\left(\left(\frac{\sigma_{xy}}{\sigma}\right)^2 + 1\right)}}$$

where $\sigma=\sigma_1$ or $\sigma=\sigma_2$

Crack inclination angle to Kr_1

$$Kr_1 = \frac{\tau_{loc}}{\sigma_{loc}} = \frac{\sigma'_{xy}}{\sigma'_{yy}} = \frac{\sigma_{yy}\cos(\theta)\sin(\theta)}{\sigma_{yy}\cos^2(\theta)} = \tan\theta = \tan(\frac{\pi}{2} - \beta)$$

where the inclined crack lies along the x' direction

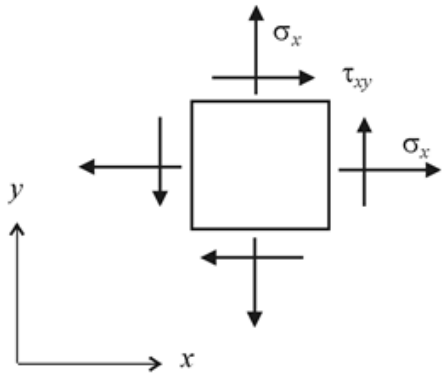

(a)

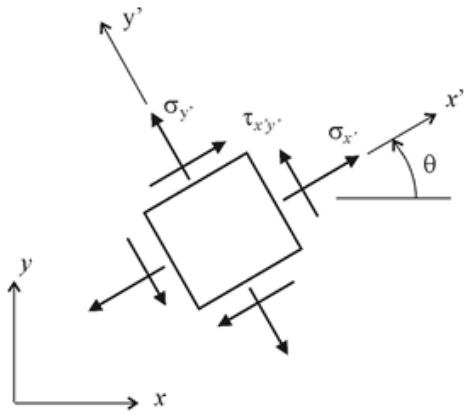

(b)

References

Banks, T. M. and Garlick, A., "The Form of Crack Tip Plastic Zones," *Engineering Fracture Mechancis*, 19, pp. 571-581 (1984).

Baxevanis, T., Chemisky, Y. and Lagoudas, D. C., "Finite element analysis of the plane strain crack-tip mechanical fields in pseudoelastic shape memory alloys." *Smart Materials and Structures*, 21(9), (2012).

Dodds, R. H., Anderson, T. L. and Kirk, M. T., "A Framwork to Correlate a/W Effects on Elastic-Plastic Fracture Toughness," *International Journal of Fracture*, 48, pp. 1-22 (1991).

Dugdale, D. S., "Yielding in Steel Sheets Containing Slits," *Journal of the Mechanics and Physics of Solids*, 8, pp. 100-104 (1960).

Erdogan, F. and Sig, G. C., "On the Crack Extension in Plates Under Plane Loading and Transverse Shear," *Journal of Basic Engineering*, 85, pp. 519-527 (1963).

Golos, K. and Wasiluk, B., "Role of Plastic Zone in Crack Growth Direction Criterion Under Mixed Mode Loading," *International Journal of Fracture*, 102, pp. 341-353 (2000).

Guerra-Rosa, L., Branco, C. M. and Radon, J. C., "Monotonic and Cyclic Crack Tip Plasticity," *International Journal of Fatigue*, 6(1), pp. 17-24 (1984).

Iida, S. and Kobayashi, A. S., "Crack Propagation Rate in 7075-T3 Plates Under Cyclic Tensile and Transverse Shear Loading," *Journal of Basic Engineering ASME Transactions*, 91, pp. 519-525 (1969).

Irwin, G., *Handbook of Physics* 6, 551-590 (1958).
Irwin, G. R., "Analysis of Stresses and Strains near the End of a Crack Traversing a Plate," *Journal of Applied Mechanics*, 24, pp. 361-364 (1957).

Jing, P., Khraishi, T. and Gorbatikh, L., "Closed-Form Solutions for the Mode II Crack Tip Plastic Zone Shape," *International Journal of Fracture*, 122(3-4), pp. L134-L142 (2003).

Jing, P., Khraishi, T. and Gorbatikh, L., "Analytic Solutions for Crack Tip Plastic Zone Shape Using the Von Mises and Tresca Yield Criteria: Effects of Crack Mode and Stress Condition," *Journal of Mechanics*, 20(3), pp. 199-210 (2004).

Khan, S. M. A., and Khraisheh, M. K., "A new Criterion for Mixed Mode Fracture Initiation Based on the Crack Tip Plastic Core Region," *International Journal of Plasticity*, 20, pp. 55-84 (2004).

Khraishi, T and Shen, Y. L., "Introductory Continuum Mechanics with Applications to Elasticity," *Cognella Inc.*, (2013).

Kong, X. M., Schluter, N. and Dahl, W., "Effect of Triaxial Stress on Mixed-Mode Fracture," *Engineering Fracture Mechanics*, 52(2), pp. 379-388 (1995).

Mishra, S. C. and Parida, B. K., "A Study of Crack-Tip Plastic Zone by Elastoplastic Finite Element Analysis," *Engineering Fracture Mechanics*, 22(6), pp. 951-956 (1985).

Theocaris, P. S., and Andrianopoulos, N.P., "The T-Criterion Applied to Ductile Fracture," *International Journal of Fracture*, 20, pp. R125-R130 (1982).

Theocaris, P. S., Kardomateas, G. A. and Andrianopoulos, N. P., "Experimental Study of the T-Criterion in Ductile Fracture," *Engineering Fracture Mechanics*, 17(5), pp. 439-447 (1982).

Unger, D. J., "A Transition Model of Crack Tip Plasticity," *International Journal of Fracture*, 44, pp. R27-R31 (1990).

Vallejo, L. E., "The Brittle and Ductile Behavior of a Material Containing a Crack Under Mixed-Mode Loading," *The 28th US Symposium on Rock Mechanics, Tucson 29 June-1 July*, pp. 383-390 (1987).

Yehia, Na, A. B., "Distortional Strain Energy Density Criterion: The Y-Criterion," *Engineering Fracture Mechanics*, 39(3) pp. 477-485 (1991).